Stopping Measles in Its Tracks: An Age-Structured SEIR-MV Model of Declining Vaccination, Waning Immunity, and Catch-Up Strategies

Ernesto Morales Carrasco

Department of Mathematics and Statistics
University of New Mexico

Submitted in fulfillment of the requirements
for the Bachelor of Science in Mathematics degree with Honors

April 2026

Thesis Advisor: Helen J. Wearing, PhD
Department of Mathematics and Statistics
University of New Mexico

Contents

Abstract

Measles remains one of the most transmissible infectious diseases known, and declining vaccination coverage has renewed the threat of large-scale outbreaks in communities once considered protected. The 2025 New Mexico measles outbreak originating in west Texas illustrates how localized coverage gaps can potentially seed wider epidemics. This thesis develops an age-structured SEIR-MV compartmental model parameterized to the New Mexico population to project measles outbreak dynamics through 2030 under four scenarios: baseline fixed vaccination coverage, declining routine coverage, targeted catch-up vaccination campaigns, and imported infections.

Under fixed coverage, the model produces inter-epidemic intervals of approximately 27 years, with the initial transient case distribution approximating the 2025 outbreak data and the effective reproduction number R_e beginning near 0.94 before oscillating around the elimination threshold of 1. When coverage declines at 0.9 percentage points per year, the first outbreak advances to year 12, peak infectious prevalence increases 3-fold, R_e dynamics compress with earlier crossings of 1, and the system transitions to endemic transmission by mid-century. Sensitivity analysis of five catch-up strategies reveals that adult first-dose campaigns achieve full epidemic suppression at approximately 500–550 vaccinations per year (driving R_e persistently below 1), while second-dose boosting of partially-immune individuals confers no measurable benefit. Under declining vaccination, no catch-up strategy achieves suppression, demonstrating how targeted campaigns cannot substitute for sustained routine immunization. Dynamic maternal immunity analysis further shows that under declining coverage, natural infection rather than vaccination becomes the dominant mechanism maintaining newborn protection.

These findings support prioritizing restoration of first-dose routine coverage above the 93–95% herd immunity threshold, with adult first-dose catch-up campaigns as the highest-yield supplementary intervention.

1 Introduction

Measles remains one of the most transmissible infectious diseases of humans, and despite the existence of a safe and effective vaccine, it continues to be a serious public health threat wherever vaccination coverage falls short. In 2025, a measles outbreak originating in an unvaccinated Mennonite community in Gaines County, west Texas, spread across the state and into neighboring Lea County, New Mexico, threatening the elimination status the United States had maintained since 2000 [8]. By mid-February 2025, Texas reported 58 cases, mostly among unvaccinated schoolchildren in home-schooled or private religious settings, while New Mexico reported 8 cases, six confirmed unvaccinated, with Gaines County's kindergarten Measles-Mumps-Rubella (MMR) vaccination rate standing at just 81%. This is well below the 93–95% coverage required to sustain herd immunity [19]. By September 2025, New Mexico alone had recorded 100 cases across 9 counties and one death, marking the state's largest measles outbreak since 1996 and its first since that year [1]. This outbreak is the local expression of a global pattern of declining vaccine coverage that, left unaddressed, makes future outbreaks increasingly likely.

A 2025 study analyzing global and WHO regional measles vaccination coverage from 2019 to 2023 found widespread declines that compromise progress toward the Immunization

Agenda 2030 (IA2030) goal of eliminating measles in at least five of six WHO regions [20]. In 2023, global mean coverage with the first and second doses of measles-containing vaccine stood at 85.2% and 77.1% respectively, with two-dose coverage averaging just 65.3% worldwide — 30% below the 95% threshold. From 2019 to 2023, global two-dose coverage fell 3.7%, and the number of zero-dose children in 2023 was 40.6% higher than levels needed to achieve a 50% reduction by 2030, with only 8.7% of countries reaching ≥95% two-dose coverage. While these trends are global in scope, they can have direct local consequences. New Mexico's own vaccination rates closely reflect this decline, and the 2025 outbreak demonstrates that coverage gaps in even a single community can seed a statewide epidemic.

What remains poorly understood, however, is how continued declines in routine vaccination coverage will interact with age-structured immunity, waning maternal protection, and the susceptibility of older unvaccinated cohorts to shape future outbreak dynamics at the state level. Existing models of measles transmission have largely focused on childhood vaccination or national-scale dynamics [4], and few have simultaneously examined the role of targeted catch-up campaigns in older age groups, the feedback between declining adult immunity and newborn maternal protection, and the sensitivity of outbreak timing to specific intervention strategies under realistic declining-coverage trajectories. While mathematical frameworks have been applied to evaluate vaccination campaign strategies in other disease contexts, such as COVID [13], their application to age-structured catch-up campaigns under declining routine coverage in a sub-national setting remains limited. This gap limits the ability of public health authorities to prioritize limited resources across age groups and intervention types when routine coverage is eroding.

Measles presents with high fever, cough, coryza, and conjunctivitis, followed by a characteristic spreading rash, and carries significant risks of severe complications including pneumonia, encephalitis, and death [5]. The disease is among the most transmissible infections known, with a basic reproduction number R_0 typically estimated between 12 and 18 [10]. Mathematical models have been crucial to understanding measles epidemiology. The foundational SEIR models [11, 15] partition populations into Susceptible, Exposed, Infectious, and Recovered compartments to describe epidemic dynamics, and the effective reproduction number under vaccination R_e quantifies how coverage translates into herd protection. The first MMR dose is recommended at 12–15 months and the second at 4–6 years [6]. Because measles exhibits one of the highest R_0 values of any infectious disease, sustaining herd protection requires an exceptionally large immune fraction. The herd immunity threshold, defined as $1 - 1/R_0$, implies that eliminating sustained transmission demands immunity in roughly 92–95% of the population [10, 3]. Achieving ≥95% two-dose MMR coverage is therefore the benchmark target set by public health authorities to maintain $R_e < 1$ and prevent future outbreaks [6].

Mathematical modeling of measles transmission has a rich history. Schenzle introduced age-structured models parameterized to case notification data, and Grenfell & Anderson demonstrated how age-specific mixing patterns drive epidemic cycles [9, 23]. Bolker & Grenfell further established how school-term forcing and contact heterogeneity shaped the characteristic biennial measles cycles observed in pre-vaccine era data [4]. The explicit incorporation of maternally-derived immunity into compartmental models was motivated by McLean & Anderson and further formalized by Hethcote [12, 18]. These foundations form the central structural features of current models.

To address the gap identified above, we develop an age-structured SEIR-MV compartmental model parameterized to the New Mexico population, incorporating time-varying vaccination coverage, age-specific contact patterns, maternal antibody decay, and targeted catch-up intervention scenarios to project outbreak dynamics through the next few decades. The model is designed to answer four specific questions. First, if New Mexico vaccination trends continue to mirror the observed global decline of 3.7% over 2019–2023, what are the projected size and age-specific burden of future outbreaks? Second, how effective are targeted catch-up vaccination campaigns in older age groups relative to sustaining routine childhood coverage, and how many individuals must be vaccinated annually to achieve meaningful outbreak suppression? Third, what are the implications of declining adult vaccination coverage for the dynamic loss of maternal immunity and its downstream effects on infant vulnerability? Finally, how do these dynamics hold when imported infections are introduced?

2 Methods

2.1 Model Overview

A compartmental model partitions a population into discrete classes, called *compartments*, and tracks the flow of individuals between them over time using a system of differential equations. The classical SEIR framework uses four epidemiological compartments: Susceptible (S), Exposed (E), Infectious (I), and Recovered (R), where individuals progress through each stage as an infection unfolds. Transitions between compartments are governed by the rate of new infections being proportional to the product of the susceptible and infectious populations [14]. Building on this framework, we construct an age-structured SEIR-MV model parameterized to measles transmission for the recent New Mexico epidemic. The population is subdivided in two ways: by *age group* and by *infection status*. The four age groups are newborns (0–1 years), toddlers (1–5 years), kids and teenagers (5–19 years), and adults (20 years and older), indexed $k = 0, 1, 2, 3$ respectively. Within each age group, individuals are further classified by their infection and immune status into one of the following compartments: S_k (fully susceptible), E_k (exposed but not yet infectious), I_k (actively infectious), R_k (recovered or fully immune), M_0 (newborns carrying transplacentally acquired maternal antibodies, which wane over the first months of life), and V_k (partially immune individuals who have received only the first dose of the MMR vaccine). Individuals can progress to R_k upon receiving the second MMR dose or through natural recovery from infection. The M and V compartments are considered partially immune. Figure 1 provides an illustration of the SEIR-MV model, where columns represent infection status and rows represent age groups.

2.2 Routine Vaccination

The susceptible compartment, denoted as S, consists of the population that remains vulnerable to infection but has not yet been exposed. New individuals continuously enter S_0 through births at a rate given by $\mu_B N$, where μ_B represents the natural birth rate and N is the total population size. However, only a fraction $(1 - \rho)$ of these newborns enters the

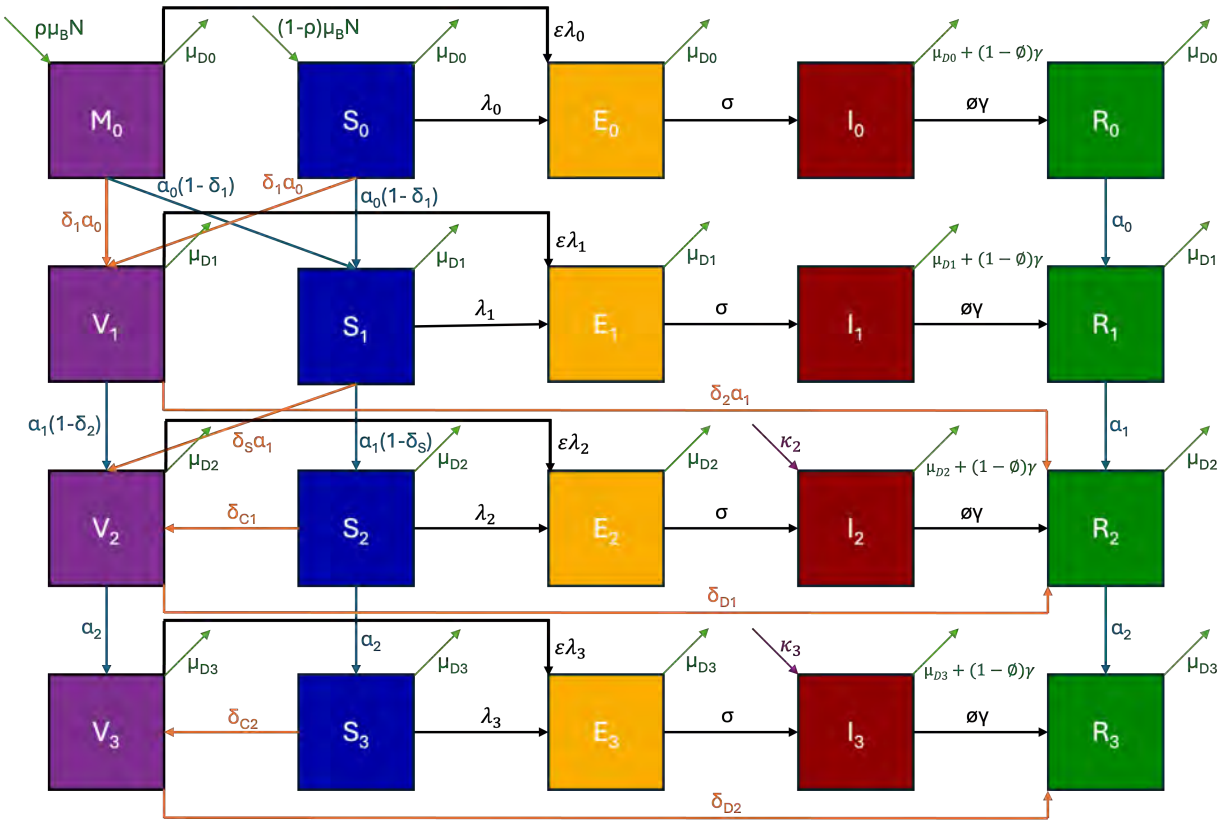

Figure 1: SEIR-MV Model Diagram. Each box represents a compartment tracking the number of individuals in that class at time t. Compartment classes are: S – Susceptible (fully), E – Exposed, I – Infectious, R – Recovered/Fully Immune, M_0 – Partially immune newborns with waning maternal immunity, V – Partially immune with single-dose of the MMR. Indices 0, 1, 2, 3 correspond to age groups 0–1, 1–5, 5–19, and 20+ years respectively. Newborns enter M_0 at rate $\rho\mu_B N$ and S_0 at rate $(1-\rho)\mu_B N$. Green upward diagonal arrows denote natural (μ_{Dk}) and disease-induced mortality ($(1-\phi)\gamma$ from the infectious classes only), through which individuals permanently exit the population. Blue arrows denote aging between age groups at rate α_k. Black arrows denote progression through infection stages via the force of infection λ_k (or $\varepsilon\lambda_k$ for partially immune compartments), with infectious individuals recovering into R_k at rate $\phi\gamma$ or dying from disease at rate $(1-\phi)\gamma$, reflected in the outgoing arrows from I_k. Orange arrows denote routine and catch-up vaccination flows moving susceptible or partially immune individuals into higher immunity classes. Pink arrows denote imported infections into the older age groups. The force of infection $\lambda_k = \sum_{j=0}^{3} \beta_{kj} I_j / N$ is governed by the 4×4 WAIFW transmission matrix $\boldsymbol{\beta}$, whose (k, j) entry gives the transmission rate from infectious individuals in age group j to susceptibles in age group k.

susceptible class, while ρ represents the proportion born with immunity from maternal antibodies who enter the M-class. Due to the waning nature of maternal immunity, all newborns age into either the toddler's V_1 or S_1 class. Newborns age into V_1 at the rate $\delta_1\alpha_0$, where δ_1 represents the fraction of newborns who receive their first MMR dose at 12 months old. The remaining newborns age into S_1 at the rate $\alpha_0(1-\delta_1)$. Toddlers who have already received their first dose can receive their second dose and age into the R_2-class at the rate $\delta_2\alpha_1$, or

remain in the V-class and age into V_2 at the rate $\alpha_1(1-\delta_2)$ if no such dose is received.

2.3 Transmission & Infection Process

The force of infection (i.e. the rate at which susceptible individuals become infected) at time t for group k is defined as:

$$\lambda_k(t) = \sum_{j=0}^{3} \beta_{kj} \frac{I_j(t)}{N}, \qquad k = 0, 1, 2, 3 \tag{1}$$

where $I_j(t)$ denotes the number of infectious individuals in age group j at time t, β_{kj} is the transmission rate from infectious group j to susceptible group k, and $N = N(t)$ is the total population size at time t. Therefore, $I_j(t)/N$ reflects the proportion of the population that is infectious in age group j. Similarly, the rate at which partially-immune individuals become infected occurs at the rate $\varepsilon\lambda_k(t)$, where $0 < \varepsilon \ll 1$ due to the observation that partial immunity can greatly reduce the chance of infection, but not to zero. Transmission rate values vary between age groups; therefore all β_{kj}'s are indexed and organized into a WAIFW contact matrix (Who Acquired Infection From Whom). Because measles includes a latent period, new infections first move to the exposed compartment E, which contains individuals who have been infected but are not yet capable of transmitting the infection. Exposed individuals transition to the infectious state at rate σ, the reciprocal of the average latent period. The infectious compartment I includes those who are actively infected and able to spread the infection to others. Of these, a fraction ϕ survive and recover into the recovered compartment R at rate γ, while the remaining fraction $(1-\phi)$ die from the infection at the same rate γ. This parameterization reflects the assumption that disease-induced death and recovery occur on the same timescale, with the outcome determined by ϕ. Consequently, the effective recovery rate is $\phi\gamma$ and the disease-induced death rate is $(1-\phi)\gamma$. The R-class consists of individuals who have either recovered from the infection and gained immunity, or received both doses of the MMR vaccine. Across all compartments, μ_{Dk} denotes the natural death rate from non-disease causes in age group k.

2.4 Targeted Treatment

Susceptible toddlers can receive a late first dose and age into the V_2-class at the rate $\delta_S\alpha_1$, while the remaining age into S_2 at the rate $\alpha_1(1-\delta_S)$. The remaining catch-up vaccination campaigns will be modeled in the latter two age groups, where susceptible teenagers and adults can receive a first "catch-up" MMR dose at the rate δ_C and move into the V-class within their respective age group. The partially-immune individuals can then receive their second "catch-up" MMR dose at the rate δ_D and move into the R-class within their respective age group. The model assumes individuals age only in the susceptible, partial immunity, and recovered/fully-immune classes, because the duration of infection (in days) is relatively short compared to the duration of an age class (in years).

2.5 Imported Infections

To assess the sensitivity of the model to external transmission pressure, imported infections are incorporated via additive terms κ_k in the infectious compartments of the two oldest age groups (see Equations (15) and (20)). Imported infections are not applied to the infant ($k = 0$) or toddler ($k = 1$) groups, as travel-related importation is considered most epidemiologically relevant among school-age individuals and adults; accordingly, $\kappa_0 = \kappa_1 = 0$ throughout and are not included in the model equations. Each κ_k represents a constant daily rate of infectious individuals entering from outside the modeled population. In the baseline scenario, imported infections are disabled ($\kappa_2 = \kappa_3 = 0$). Results are compared under both the no-importation baseline and an activated importation scenario to evaluate how external seeding pressure affects outbreak dynamics and the efficacy of catch-up vaccination campaigns.

2.6 System of Differential Equations

Since each compartment represents a non-negative population size, we require M_0, V_j, $S_k, E_k, I_k, R_k \geq 0$ for all $t \geq 0$ and $j = 1, 2, 3$, $k = 0, 1, 2, 3$. The right-hand side of each equation is constructed so that outflow terms vanish when the corresponding state variable is zero, ensuring the system is positively invariant and all state variables remain non-negative for non-negative initial conditions [2, 15, 16]. We obtain a system of ordinary differential equations, which are integrated numerically using MATLAB's `ode45` solver, an explicit Runge-Kutta method.

The model tracks four age groups (indexed $k = 0, 1, 2, 3$), where $k = 0$ corresponds to infants aged 0–1 years, $k = 1$ to children aged 1–5 years, $k = 2$ to individuals aged 5–19 years, and $k = 3$ to adults aged 20 years and older. Each group contains compartments S, E, I, R, and M or V.

Group 0: Newborns (0–1 years)

$$\frac{dM_0}{dt} = \rho\,\mu_{\text{birth}} N - \alpha_0 M_0 - \varepsilon\lambda_0 M_0 - \mu_{D0} M_0 \tag{2}$$

$$\frac{dS_0}{dt} = (1-\rho)\,\mu_{\text{birth}} N - \lambda_0 S_0 - \alpha_0 S_0 - \mu_{D0} S_0 \tag{3}$$

$$\frac{dE_0}{dt} = \varepsilon\lambda_0 M_0 + \lambda_0 S_0 - \sigma E_0 - \mu_{D0} E_0 \tag{4}$$

$$\frac{dI_0}{dt} = \sigma E_0 - \gamma I_0 - \mu_{D0} I_0 \tag{5}$$

$$\frac{dR_0}{dt} = \phi\,\gamma I_0 - \alpha_0 R_0 - \mu_{D0} R_0 \tag{6}$$

Group 1: Toddlers (1–5 years)

$$\frac{dV_1}{dt} = \delta_1\alpha_0 M_0 + \alpha_0\delta_1 S_0 - \varepsilon\lambda_1 V_1 - \alpha_1 V_1 - \mu_{D1} V_1 \tag{7}$$

$$\frac{dS_1}{dt} = \alpha_0(1-\delta_1)(M_0 + S_0) - \lambda_1 S_1 - \alpha_1 S_1 - \mu_{D1} S_1 \tag{8}$$

$$\frac{dE_1}{dt} = \varepsilon\lambda_1 V_1 + \lambda_1 S_1 - \sigma E_1 - \mu_{D1} E_1 \tag{9}$$

$$\frac{dI_1}{dt} = \sigma E_1 - \gamma I_1 - \mu_{D1} I_1 \tag{10}$$

$$\frac{dR_1}{dt} = \phi\,\gamma I_1 + \alpha_0 R_0 - \alpha_1 R_1 - \mu_{D1} R_1 \tag{11}$$

Group 2: Kids & Teenagers (5–19 years)

$$\frac{dV_2}{dt} = \alpha_1(1-\delta_2)V_1 + \alpha_1\delta_S S_1 + \delta_{C_1} S_2 - \varepsilon\lambda_2 V_2 - \alpha_2 V_2 - \delta_{D_1} V_2 - \mu_{D2} V_2 \tag{12}$$

$$\frac{dS_2}{dt} = \alpha_1(1-\delta_S)S_1 - \lambda_2 S_2 - \delta_{C_1} S_2 - \alpha_2 S_2 - \mu_{D2} S_2 \tag{13}$$

$$\frac{dE_2}{dt} = \varepsilon\lambda_2 V_2 + \lambda_2 S_2 - \sigma E_2 - \mu_{D2} E_2 \tag{14}$$

$$\frac{dI_2}{dt} = \sigma E_2 - \gamma I_2 - \mu_{D2} I_2 + \kappa_2 \tag{15}$$

$$\frac{dR_2}{dt} = \phi\,\gamma I_2 + \alpha_1\delta_2 V_1 + \delta_{D_1} V_2 + \alpha_1 R_1 - \alpha_2 R_2 - \mu_{D2} R_2 \tag{16}$$

Group 3: Adults (20+ years)

$$\frac{dV_3}{dt} = \alpha_2 V_2 + \delta_{C_2} S_3 - \varepsilon\lambda_3 V_3 - \delta_{D_2} V_3 - \mu_{D3} V_3 \tag{17}$$

$$\frac{dS_3}{dt} = \alpha_2 S_2 - \lambda_3 S_3 - \delta_{C_2} S_3 - \mu_{D3} S_3 \tag{18}$$

$$\frac{dE_3}{dt} = \varepsilon\lambda_3 V_3 + \lambda_3 S_3 - \sigma E_3 - \mu_{D3} E_3 \tag{19}$$

$$\frac{dI_3}{dt} = \sigma E_3 - \gamma I_3 - \mu_{D3} I_3 + \kappa_3 \tag{20}$$

$$\frac{dR_3}{dt} = \phi\,\gamma I_3 + \alpha_2 R_2 + \delta_{D_2} V_3 - \mu_{D3} R_3 \tag{21}$$

Total Population Size

The total population N at time t is computed dynamically as the sum of all 20 state compartments:

$$N = \sum_{k=0}^{3}(S_k + E_k + I_k + R_k) + M_0 + \sum_{k=1}^{3} V_k \tag{22}$$

Because births, deaths, and disease-induced mortality all operate continuously throughout the simulation, $N = N(t)$ is not held fixed but evolves naturally as a consequence of differences between the birth and death rate parameters. Note that $N(t)$ is a derived quantity computed from the state variables at each time step and is not an independent model parameter.

Cumulative Cases

To track cumulative disease burden over the simulation period, we augment the system of differential equations with four cumulative case compartments C_k, one per age group:

$$\frac{dC_0}{dt} = \gamma I_0 \tag{23}$$

$$\frac{dC_1}{dt} = \gamma I_1 \tag{24}$$

$$\frac{dC_2}{dt} = \gamma I_2 \tag{25}$$

$$\frac{dC_3}{dt} = \gamma I_3 \tag{26}$$

These compartments are initialized to zero and accumulate the total flow out of each infectious class over time, following the approach described in Keeling & Rohani [15] (pg. 51). Because γI_k represents the rate at which infectious individuals exit the I_k compartment, integrating this quantity yields the total number of individuals who completed an infectious period, which serves as our measure of total reported cases per age group.

At the end of the simulation, age-group case counts are read directly from the terminal values $C_k(t_{\text{final}})$ and rounded to the nearest integer. Total cases across all age groups are then computed as:

$$C_{\text{total}} = C_0 + C_1 + C_2 + C_3. \tag{27}$$

This calculation separates cumulative incidence from the active infectious compartment which allows for outbreak size to be quantified independently at any given time point.

2.7 Parameter Descriptions

Parameter	Description
μ_{birth}	Per-capita birth rate
μ_{Dk}	Background per-capita mortality rate in age group k
ρ	Fraction of births receiving maternal immunity
α_k	Aging/transition rate out of age group k
δ_1, δ_2	Vaccination probability at first and second dose transitions
δ_S	Early catch-up vaccination probability
$\delta_{C_1}, \delta_{C_2}$	Catch-up first dose vaccination rate in age groups 2 and 3
$\delta_{D_1}, \delta_{D_2}$	Catch-up second dose vaccination rate in age groups 2 and 3
ε	Susceptibility reduction in vaccinated class V $(0 \leq \varepsilon \leq 1)$
β_{kj}	Transmission rate from age group j to age group k
σ	Rate of progression from exposed to infectious class
γ	Recovery rate
ϕ	Probability of surviving infection $(= 1 - p$, the probability of dying from measles)
κ_2, κ_3	Imported infection rate in age groups 2 and 3

2.8 Parameterization

2.8.1 Demographics

The model is parameterized to reflect the New Mexico population using 2023 CDC data, with all rates expressed in units of days; this was due to 2023 data being the most accessible. The per-capita birth rate is set to $\mu_{\text{birth}} = 10.9/1000/365$ per day, corresponding to New Mexico's reported birth rate of 10.9 births per 1,000 individuals annually. Age-group-specific mortality rates μ_{Dk} are estimated using weighted averages from New Mexico life-table data [17]. Infant and toddler mortality (groups 0 and 1) share a rate of $\mu_0 = \mu_1 = 1/(771 \times 365)$ per day, while the school-age group contains a lower mortality of $\mu_2 = 1/(2{,}650 \times 365)$ per day. Adult mortality is set to $\mu_3 = 1/(87.76 \times 365)$ per day.

Aging rates α_k govern the flow of individuals from one age group to the next and are taken as the reciprocal of the number of days spent in each group: $\alpha_0 = 1/365$ per day (infants spend 1 year in group 0), $\alpha_1 = 1/(4 \times 365)$ per day (toddlers spend 4 years in group 1), and $\alpha_2 = 1/(14 \times 365)$ per day (the school-age group spans 14 years before aging into adulthood).

2.8.2 Transmission

Transmission between age groups is governed by the 4×4 WAIFW (Who Acquires Infection From Whom) matrix $\boldsymbol{\beta}$, whose entries β_{kj} represent the transmission rate from infectious individuals in age group j to susceptibles in age group k. The matrix is parameterized following the approach of Bolker and Keeling & Rohani [15, 4], with age-specific values estimated from England and Wales contact data. The resulting values, scaled by a factor of 1.112 to calibrate initial transient infection levels to the 2025 New Mexico outbreak, are:

$$B_0 = B_1 \approx 4.6490, \quad B_2 \approx 2.7927, \quad B_3 \approx 2.7961 \quad \text{(per day)}.$$

The matrix is structured so that within-group contact is highest among infants and young children and declines with age:

$$\boldsymbol{\beta} = \begin{pmatrix} B_0 & B_1 & B_2 & B_3 \\ B_1 & B_1 & B_2 & B_3 \\ B_2 & B_2 & B_2 & B_3 \\ B_3 & B_3 & B_3 & B_3 \end{pmatrix}. \tag{28}$$

2.8.3 Infection and Recovery

The latent period and infectious period are taken from Keeling & Rohani [15] and are assumed uniform across age groups. The rate of progression from the exposed to infectious compartment is $\sigma = 1/8$, corresponding to a mean latent period of 8 days. The recovery rate is $\gamma = 1/5$ per day, corresponding to a mean infectious period of 5 days. The infection survival probability is $\phi = 1 - p$, where $p = 0.001$ is the age-averaged case fatality ratio for measles [5].

The partial-immunity susceptibility parameter ε governs the reduced but nonzero probability of infection for individuals in the M and V compartments. This is set uniformly across age groups to $\varepsilon = 0.07$, derived as the probability that a partially immune individual becomes infected upon exposure [6].

2.8.4 Vaccination

Routine vaccination parameters are derived from weighted New Mexico county-level coverage estimates for 2025 [1]. The first-dose coverage probability is $\delta_1 = 0.9238$, representing the weighted fraction of infants who successfully receive the first MMR dose before aging out of group 0. This same value is used for ρ, the fraction of newborns assumed to carry maternal antibodies. The second-dose coverage probability is $\delta_2 = 0.7424$, representing the fraction of V_1 toddlers who receive the second MMR dose before aging into group 2. The early catch-up dose probability δ_S and later catch-up dose rates $\delta_{C1}, \delta_{D1}, \delta_{C2}, \delta_{D2}$ are set to zero in the baseline to be experimented with later.

2.8.5 Imported Infections

When activated, κ_k is parameterized as

$$\kappa_k = \frac{n_k}{365 \cdot \tau_k}, \tag{29}$$

where $k \in \{2, 3\}$ and $n_k \in \mathbb{N}$ is the number of imported cases per event in groups k_2, k_3 and τ_k is the average number of years between imported cases. In the baseline scenario, imported infections are disabled ($\kappa_2 = \kappa_3 = 0$).

2.9 Effective Reproduction Number

Entries R_{kj} of the next generation matrix (NGM) define the average number of secondary infections in age group k generated by a primary infection in age group j [7, 15]. Because our

model is initialized with susceptible, vaccinated, and immunized individuals, the dominant eigenvalue of this matrix corresponds to the *effective* reproduction number of the system, R_e, the average number of secondary infections generated by a typical primary infection in a population of susceptible and non-susceptible hosts. The NGM is given by

$$\begin{pmatrix} R_{00} & R_{01} & R_{02} & R_{03} \\ R_{10} & R_{11} & R_{12} & R_{13} \\ R_{20} & R_{21} & R_{22} & R_{23} \\ R_{30} & R_{31} & R_{32} & R_{33} \end{pmatrix} \tag{30}$$

where

$$R_{0j} = \frac{\sigma\beta_{0j}}{(\sigma+\mu_{Dj})(\gamma+\mu_{Dj})}\left[\frac{S_0}{N} + \varepsilon\frac{M_0}{N}\right] \tag{31}$$

for $j = 0, 1, 2, 3$, and

$$R_{kj} = \frac{\sigma\beta_{kj}}{(\sigma+\mu_{Dj})(\gamma+\mu_{Dj})}\left[\frac{S_k}{N} + \varepsilon\frac{V_k}{N}\right] \tag{32}$$

for $k = 1, 2, 3$ and $j = 0, 1, 2, 3$. Note that the S_ks, M_0 and V_ks represent populations of newborns with maternal antibodies, fully susceptible individuals in age group k and partially vaccinated individuals in age group k, respectively.

Intuitively, each entry of the NGM is the product of the fraction of infected individuals of type j surviving the exposed class ($\frac{\sigma}{\sigma+\mu_{Dj}}$), the number of new infections of type k generated by infectious type j per unit time (e.g. $\beta_{0j}[\frac{S_0}{N} + \epsilon\frac{M_0}{N}]$ for $k = 0$) and the average duration of effective infectiousness of type j ($\frac{1}{\gamma+\mu_{Dj}}$).

In this analysis, we computed R_e dynamically across the simulation window for the baseline case, the declining vaccination scenario, and the full range of vaccination campaigns.

2.10 Initial Conditions

Initial conditions are set to reflect the New Mexico population distribution in 2023, with individuals allocated across compartments based on age-group census estimates and vaccination coverage data. The initial values (at $t = 0$) of the state variables are given by:

$$\begin{aligned} (M_0(0),\, S_0(0),\, E_0(0),\, I_0(0),\, R_0(0)) &= (26449,\ 2183,\ 0,\ 2,\ 0), \\ (V_1(0),\, S_1(0),\, E_1(0),\, I_1(0),\, R_1(0)) &= (79345,\ 6549,\ 0,\ 2,\ 0), \\ (V_2(0),\, S_2(0),\, E_2(0),\, I_2(0),\, R_2(0)) &= (75587,\ 31781,\ 0,\ 1,\ 309452), \\ (V_3(0),\, S_3(0),\, E_3(0),\, I_3(0),\, R_3(0)) &= (218947,\ 73147,\ 0,\ 0,\ 1303011). \end{aligned} \tag{33}$$

There are no immune infants with a second dose of the MMR vaccine, so all immune infants start in M_0. Similarly, the toddler group carries no initial recovered individuals ($R_1 = 0$), as the model assumes toddlers who receive a second MMR dose age directly into the R_2 compartment rather than remaining in group 1, so all immune toddlers are captured in V_1. The adults were initialized with a redistribution of 40% of V_3 and 20% of S_3 estimates moved into the recovered pool R_3 to better capture the 2025 epidemic. Due to uncertainty in adult immune status from lack of historical seropositive data for New Mexico, we can assume there are more immune adults than recorded. Once the model's demographic parameters

were calibrated to a non-infectious population, exposed compartments are initialized to zero across all age groups and infectious compartments are seeded with small nonzero values ($I_0 = I_1 = 2$, $I_2 = 1$, $I_3 = 0$) to initiate transmission at the start of the simulation. The four cumulative case compartments C_0, C_1, C_2, C_3 are initialized to zero.

2.11 Detecting Epidemic Years

To systematically detect and record epidemic events across simulation scenarios, we implement a peak-detection algorithm applied to the total infectious signal combined across all age groups:

$$I_{\text{total}}(t) = I_0(t) + I_1(t) + I_2(t) + I_3(t). \tag{34}$$

A local maximum in I_{total} is classified as an epidemic peak if it exceeds a minimum peak size threshold of 5% of the global maximum of I_{total} over the simulation horizon (this filters out minor fluctuations). To avoid misclassifying the initial seeding transient as an epidemic event, all peaks occurring before year 2 of the simulation are discarded. Additionally, to prevent double counting a single outbreak, peaks within 3 years of one another are merged by retaining only the tallest peak within each window.

Formally, a time t^* is recorded as an epidemic year if:

$$I_{\text{total}}(t^*) > I_{\text{total}}(t^* \pm \Delta t) \quad \text{and} \quad I_{\text{total}}(t^*) > 0.05 \cdot \max_t I_{\text{total}}(t), \quad t^* \geq 2 \text{ years}. \tag{35}$$

The surviving peaks are sorted chronologically and the first entry is taken as the first epidemic year T, which serves as the primary outcome variable in the sensitivity analysis of Section 2.13. If no qualifying peak is detected within the simulation window, the simulation is classified as suppressive and T is assigned the value of the simulation endpoint.

2.12 Declining Vaccination

To simulate the trajectory of measles vaccination coverage under continued global decline, the first and second routine dose vaccination rates are modeled as time-varying parameters rather than fixed constants. Motivated by the 3.7% global decline in two-dose coverage observed between 2019 and 2023, both δ_1 and δ_2 are assumed to decrease linearly over the simulation period at a rate of 0.9 percentage points per year:

$$\delta_1(t) = \max\left(\delta_1 - \frac{0.009}{365}\,t,\ 0.8338\right), \qquad \delta_2(t) = \max\left(\delta_2 - \frac{0.009}{365}\,t,\ 0.6524\right), \tag{36}$$

where t is measured in days, $\delta_1 = 0.9238$ and $\delta_2 = 0.7424$ are the baseline values, and the max operator enforces floor values of 0.8338 and 0.6524 for the first and second doses respectively. These floors represent a reasonable lower bound on coverage, assuming the yearly 0.9% decrease in vaccination occurs for only 10 years after the start of the simulation.

The time-varying rates $\delta_1(t)$ and $\delta_2(t)$ enter the model by replacing the fixed parameters δ_1 and δ_2 in the M_0, S_0, V_1, S_1, V_2, and R_2 equations at each integration step, so that the effective vaccination pressure on the newborn and toddler cohorts declines continuously over the projection horizon. All other parameters remain fixed. This scenario is compared against the baseline fixed-coverage scenario to quantify the projected increase in outbreak size attributable to declining routine immunization.

2.13 Vaccination Campaigns

To evaluate the effectiveness of targeted catch-up vaccination as a complement to baseline or declining routine immunization, we perform a sensitivity analysis examining five distinct campaign strategies across the three oldest age groups. Each strategy corresponds to a single catch-up vaccination parameter being activated in isolation while all others are held at zero so the impact of each intervention can be identified independently.

The five strategies considered are:

1. δ_S: a late first-dose catch-up targeting susceptible toddlers in group 1.
2. δ_{C_1}: a first-dose catch-up targeting susceptible teenagers in group 2.
3. δ_{C_2}: a first-dose catch-up targeting susceptible adults in group 3.
4. δ_{D_1}: a second-dose catch-up targeting single-vaccinated teenagers in V_2.
5. δ_{D_2}: a second-dose catch-up targeting single-vaccinated adults in V_3.

For each strategy, the campaign is parameterized in terms of the number of vaccinations administered per year, swept over the range $\{0, 50, 100, \ldots, 800\}$ vaccinations per year. The corresponding per-capita daily rates are obtained by dividing the annual campaign size by the relevant susceptible or partial-immunity populations at baseline:

$$\delta_{C_1} = \frac{n}{365 \cdot S_2(0)}, \qquad \delta_{C_2} = \frac{n}{365 \cdot S_3(0)}, \tag{37}$$

$$\delta_{D_1} = \frac{n}{365 \cdot V_2(0)}, \qquad \delta_{D_2} = \frac{n}{365 \cdot V_3(0)}, \tag{38}$$

where n denotes the annual campaign size and $S_k(0)$, $V_k(0)$ are the baseline population sizes taken from the 2023 New Mexico initial conditions. The toddler catch-up rate δ_S is instead treated as a direct proportion of the susceptible toddler population rather than a per-capita daily rate (recall this term contains an aging rate), and is computed as

$$\delta_S = \frac{n}{S_1(0)} \, . \tag{39}$$

In addition to the catch-up campaign investigation, a separate sensitivity analysis is performed over the two routine dose coverage parameters δ_1 and δ_2. Rather than being parameterized in terms of vaccinations per year, these are swept as percentage-point increases above their baseline values.

For each campaign level, the model is integrated over the full simulation horizon using `ode45`, and the first epidemic year is recorded using the method from Section 2.11. If no epidemic is detected within the simulation window, the campaign is classified as suppressive at that level. Local sensitivity is then approximated with finite differences between consecutive campaign levels:

$$\frac{\Delta T}{\Delta n} = \frac{T(n_{i+1}) - T(n_i)}{n_{i+1} - n_i}, \tag{40}$$

where $T(n)$ denotes the first epidemic year under a campaign of size n vaccinations per year. Results are visualized as curves of first epidemic year against campaign size, and tables are shown for sensitivity values.

2.14 Dynamic Maternal Immunity

In the baseline model, the fraction of newborns entering the M_0 compartment with transplacentally acquired maternal antibodies is treated as a fixed parameter $\rho = \delta_1 = 0.9238$, under the assumption that maternal immune status is approximated by first-dose coverage in the population. To investigate the implications of declining vaccination coverage on newborn protection, we replace this fixed value with a dynamic formulation, $\rho(t)$, which is computed from the current immune composition of the adult population.

Specifically, $\rho(t)$ is defined as the fraction of adult women who are either single-dose vaccinated or fully recovered. This represents the proportion of mothers capable of conferring passive immunity to their newborns:

$$\rho(t) = \frac{V_3(t) + R_3(t)}{N_3(t)}, \tag{41}$$

where $N_3(t) = V_3 + S_3 + E_3 + I_3 + R_3$ is the total adult population at time t. Note the approximate evenly split proportion of men and women in the population allows us to use the entire adult population for our calculation. This creates a feedback between adult immune decay and infant vulnerability that is absent in the fixed-ρ formulation.

This dynamic form of $\rho(t)$ is tracked post-simulation by recomputing the equation above from the `ode45` solution matrix and plotted over the simulation horizon to visualize the rate at which maternal protection is disturbed under different scenarios. All other model equations remain identical, with the only structural modification being the replacement of the scalar ρ with the time-varying quantity $\rho(t)$ evaluated dynamically at each integration step.

3 Results

3.1 Model Calibration

To verify that the model is correctly implemented before introducing infection dynamics, we simulate the system with all infectious compartments set to zero and confirm that the demographic and vaccination structure behaves as expected over a 100-year time frame. Specifically, we check that each age group's compartments evolve smoothly, the exposed and infectious classes remain identically zero throughout, cumulative cases remain at zero, and the total population $N(t)$ grows at a reasonable rate with New Mexico's birth and death parameters. Figure A.1 displays the total population and compartment log-scaled trajectories for all four age groups under the no-infection calibration run, and confirm correct implementation.

3.2 Baseline Dynamics

Using the initial conditions from Section 2.10 and fixed New Mexico vaccination parameters, we simulate the full SEIR-MV model over a 100-year horizon to establish baseline epidemic behavior prior to any vaccination decline or catch-up intervention.

3.2.1 Age-Group Compartment Dynamics

Figure A.2 shows the total population and compartment log-scaled trajectories for all four age groups under baseline conditions. Unlike the no-infection calibration run, the disease compartments now exhibit clear epidemic pulses at approximately years 28, 55, and 80, visible as small transient spikes in the E_k and I_k curves within each age group panel. The lack of significant change between the calibrated and baseline total populations confirm unperturbed demographic dynamics.

3.2.2 Epidemic Signal

Figure 2 shows the infectious class over the first five years and over a full 100-year horizon. During the initial transient dynamics, the seeded infectious individuals ($I_0 = 2$, $I_1 = 2$, $I_2 = 1$) trigger a minor pulse in infections that quickly fades out within approximately two years. The system then enters a long inter-epidemic inactive period before susceptibles accumulate sufficiently to sustain the first major outbreak near year 28. The three well-resolved epidemic peaks are better distinguished, and each peak is dominated by I_3 and I_1, with peak infectious prevalence declining from roughly 100 individuals at the first outbreak to approximately 65 at the third. Although the total population grows monotonically over the simulation horizon, the proportion of immune individuals increases after each epidemic event as individuals accumulate in the recovered compartments R_k. This progressively reduces the susceptible fraction available to sustain transmission, suppressing the size of successive outbreaks despite overall population growth. The full compartment trajectories in Figure A.2 make this accumulation of immunity visually apparent on the log scale.

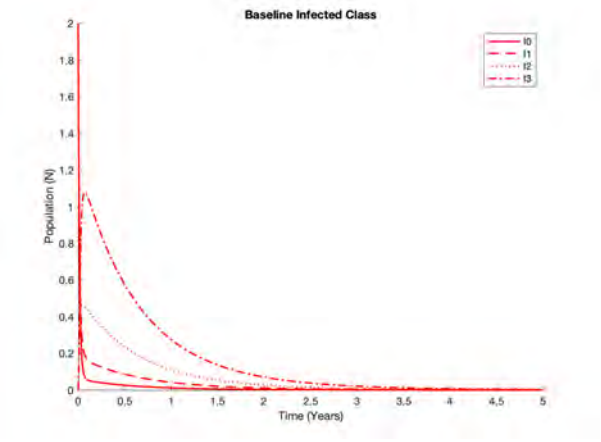

(a) Infectious compartments I_k over the first five years. The adult compartment I_3 carries the largest share of the initial infectious burden before decaying.

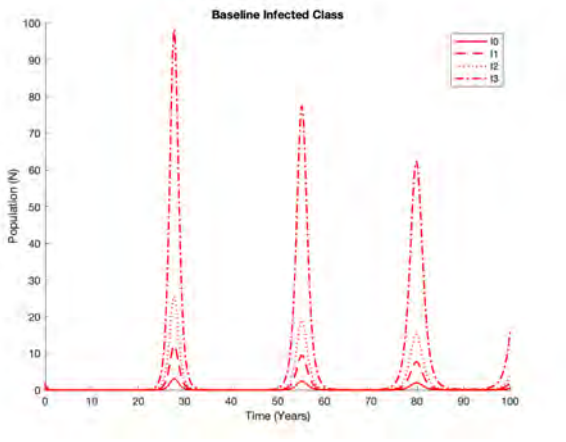

(b) Infectious compartments I_k over 100 years. Peak prevalence is dominated by adults (I_3) and toddlers (I_1) at each outbreak.

Figure 2: Infectious class trajectories under baseline conditions.

3.2.3 Cumulative Cases and Comparison with the 2025 New Mexico Outbreak

Figure 3 shows cumulative cases $C_k(t)$ by age group over both time horizons. Over 100 years, adults (C_3) accumulate the largest burden at approximately 54,000 cumulative cases, followed by teens/children (C_2) at roughly 13,500, toddlers (C_1) at roughly 6,600, and infants (C_0) at roughly 1,700. The staircase structure reflects the three discrete epidemic events at years 28, 55, and 80. Over the first five years, the initial transient produces a total of 100 modeled cases, distributed as 5 infant, 11 toddler, 25 teen/child, and 59 adult cases.

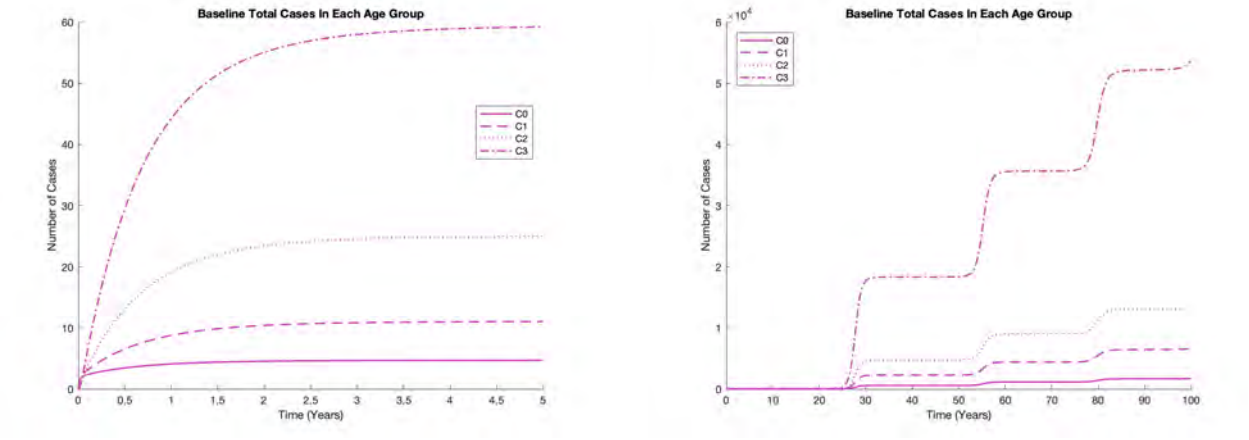

(a) Cumulative cases over the first five years. The initial transient produces 100 total cases before the system enters its inter-epidemic inactive period.

(b) Cumulative cases $C_k(t)$ over 100 years. The staircase structure reflects discrete epidemic events at years 28, 55, and 80, with adults (C_3) bearing the largest burden.

Figure 3: Cumulative cases $C_k(t)$ by age group under baseline conditions, shown over the first five years (left) and 100 years (right).

Table 1 compares the age-group distribution of the model's initial five-year case output against the confirmed case distribution from the 2025 New Mexico measles outbreak, which recorded 100 total cases across 9 counties [1].

Table 1: Comparison of modeled baseline cases (first five years) against the 2025 New Mexico outbreak case distribution by age group.

Model Age Group	NM Outbreak Age Group	Modeled Cases	2025 NM Outbreak
Groups 0–1 (0–5 years)	0–4 years	16	24
Group 2 (5–19 years)	5–17 years	25	23
Group 3 (20+ years)	18+ years	59	53
Total		100	100

While not exact, the model reproduces the broad age-group structure of the 2025 outbreak with reasonable fidelity, which provides confidence that the WAIFW transmission matrix and age-specific susceptible pool sizes are plausibly parameterized. The largest discrepancy appears in the youngest age group. The gap is likely due to the model grouping infants into a single year and toddlers into a four-year cohort. Despite this simplification, the

model's transmission dynamics produce a case distribution qualitatively similar to observed data, correctly identifying adults as the highest-burden group in New Mexico. This close agreement supports using the model for the projections in Sections 3.3–3.6.

3.2.4 Effective Reproduction Number Under Baseline Conditions

Figure 4 shows $R_e(t)$ over the full 100-year horizon under baseline fixed-coverage conditions. Beginning near 0.94 at $t = 0$, $R_e(t)$ rises as the susceptible pool accumulates, crossing the threshold $R_e = 1$ near year 10 before peaking at approximately 1.052 at the first outbreak around year 28. Following each epidemic, R_e drops sharply below 1 as susceptibles are depleted, before recovering as the population replenishes the susceptible pool through births and aging. The result is a stable sawtooth oscillation with decreasing amplitude across successive outbreaks, consistent with the epidemic peaks observed previously. The system remains near the elimination threshold throughout, confirming that the New Mexico baseline vaccination sustains a population near the boundary of herd immunity.

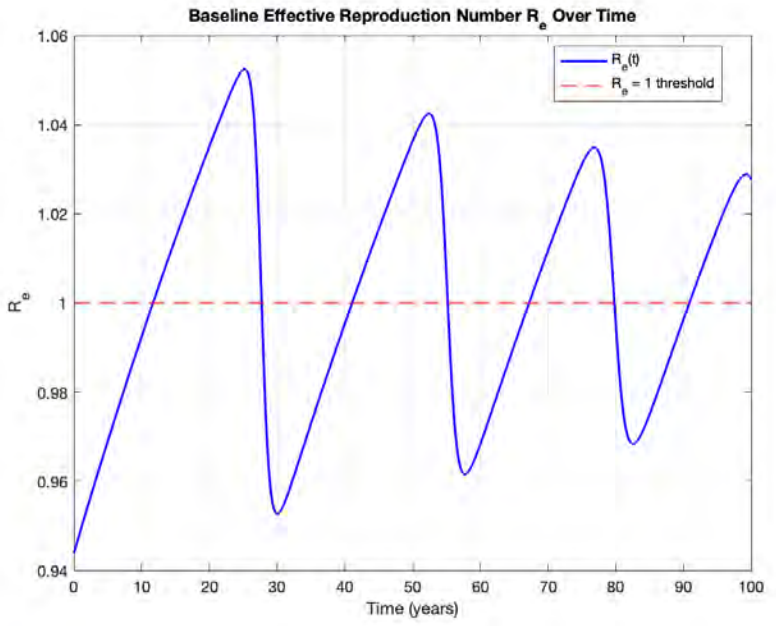

Figure 4: Effective reproduction number $R_e(t)$ under baseline fixed-coverage conditions over 100 years. The dashed red line denotes the $R_e = 1$ elimination threshold. Each upward crossing corresponds to the onset of an epidemic event, with peak R_e declining across successive outbreaks as epidemic-acquired immunity accumulates.

3.3 Projected Outbreak Dynamics Under Declining Vaccination

Under the declining vaccination scenario, both $\delta_1(t)$ and $\delta_2(t)$ decrease linearly at 0.9 percentage points per year from their 2023 baseline values for ten years as described in Section 2.12. The first outbreak occurs near year 12 rather than year 28, peak infectious prevalence is roughly three times larger, and the system never returns to the long inactive inter-epidemic

intervals characteristic of the fixed-coverage scenario. Instead, successive outbreaks compress in inter-epidemic interval and decline in peak size as epidemic-acquired immunity accumulates faster than demographic change can deplete it, eventually transitioning to a smaller-amplitude endemic oscillation by approximately year 50. The effect on epidemic dynamics is immediate and dramatic relative to the baseline.

3.3.1 Epidemic Signal and Cumulative Cases Structure

Figure 5 illustrates the dynamics of the infectious classes and total cases over a 100-year horizon. The initial outbreak, occurring shortly after year 10, reaches a peak prevalence of approximately 300 simultaneous infectious individuals, primarily driven by the adult and toddler cohorts. This represents a significant increase over the first baseline outbreak. Subsequent outbreaks occur at intervals of approximately 8–12 years. The peak prevalence of these events declines progressively as the infectious classes deplete the susceptible pools more rapidly than they can be replenished under waning vaccination coverage. By year 60, the system begins to stabilize into a sustained endemic pattern, with most age groups fluctuating between 40 and 70 individuals, while the infant class (I_0) maintains a notably lower, damped oscillation.

In contrast to the baseline pattern of discrete jumps, the declining vaccination scenario produces a continuously accelerating accumulation of cases across all age groups, signaling a transition from episodic outbreaks to sustained endemic transmission. By year 100, cumulative cases reach approximately 240,000 in adults (C_3), 105,000 in older children (C_2), 55,000 in toddlers (C_1), and 10,000 in infants (C_0). This results in a total disease burden roughly an order of magnitude greater than the baseline scenario over the same 100-year horizon, with the adults representing the vast majority of the cumulative impact.

3.3.2 Effective Reproduction Number Under Declining Vaccination

Figure 6 shows $R_e(t)$ under the declining vaccination scenario. In contrast to the baseline, the oscillations are compressed in period and damped in amplitude, with the first crossing of $R_e = 1$ occurring near year 10 and successive crossings at intervals of approximately 7–10 years thereafter. Peak R_e reaches approximately 1.05 at the first outbreak before declining progressively as epidemic-acquired immunity accumulates faster than routine vaccination decline can replenish the susceptible pool. By approximately year 50 the oscillations have damped to a narrow band centered near $R_e = 1$, consistent with the transition to endemic dynamics described previously. The convergence of R_e toward 1 from above reflects the system settling into an endemic equilibrium rather than the elimination state that would require R_e to remain persistently below 1.

3.4 Sensitivity Analysis of Catch-Up Vaccination Strategies

3.4.1 Without Declining Vaccination

Figure 7 and Table 2 display results for the sensitivity of the first epidemic year, T, to catch-up campaign size across all five strategies, without importation or declining vaccination.

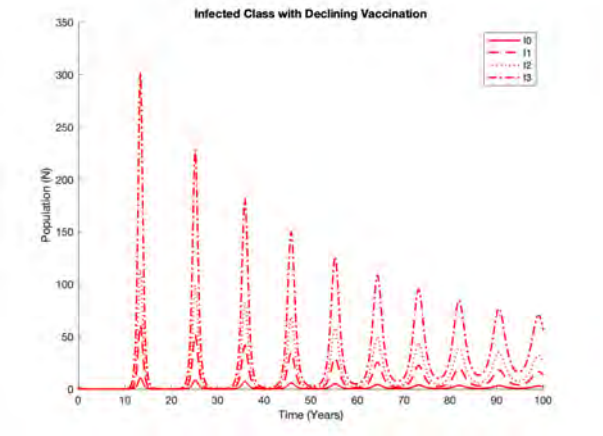

(a) Infectious compartments I_k over 100 years. The model exhibits large initial outbreaks followed by dampening oscillations, eventually converging toward an endemic steady state between years 80 and 100. Adults (I_3) and toddlers (I_1) consistently drive the peak prevalence across all cycles.

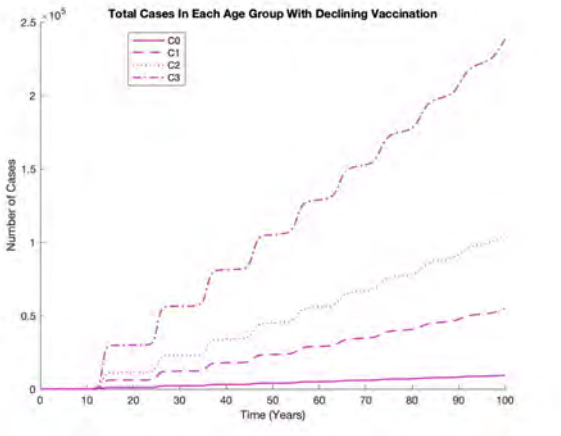

(b) Cumulative cases $C_k(t)$ by age group under declining vaccination over 100 years. The erosion of vaccination coverage leads to a shift from the discrete, "staircase" accumulation seen in baseline scenarios to a continuously accelerating growth pattern. By year 100, the total disease burden is significantly higher than baseline.

Figure 5: Infectious class and total cases trajectories under declining vaccination over 100 years.

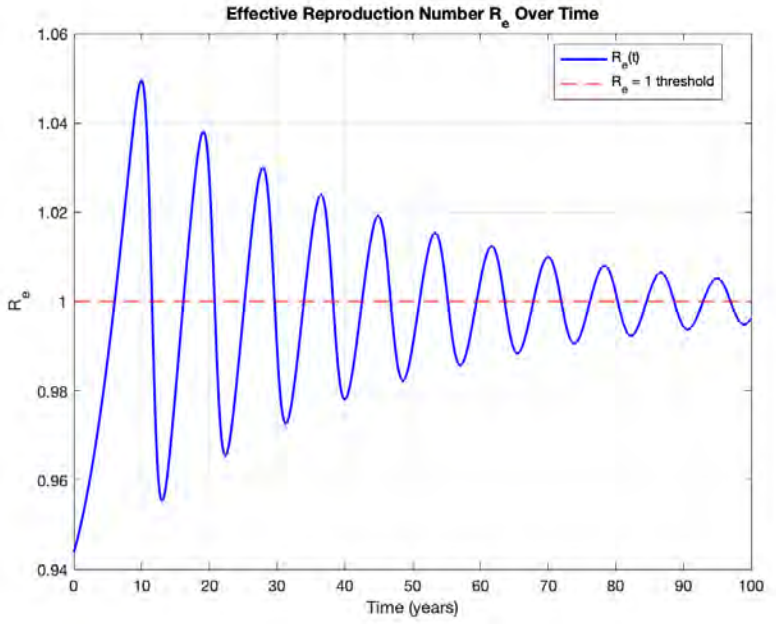

Figure 6: Effective reproduction number $R_e(t)$ under declining vaccination over 100 years. The dashed red line denotes the $R_e = 1$ threshold. Compared to the baseline, outbreaks occur earlier and at shorter intervals, with oscillations damping toward a narrow endemic band near $R_e = 1$ by approximately year 50.

The five strategies exhibit different dose-response profiles, falling into three broad behavioral

categories.

The two first-dose catch-up campaigns targeting older age groups demonstrated the strongest capacity to delay and ultimately suppress epidemics. Adult first-dose catch-up (δ_{C_2}) was the most efficient intervention, achieving full suppression (at the simulation endpoint of 100 years) at a campaign size of approximately 550 vaccinations per year. Teen first-dose catch-up (δ_{C_1}) followed a similar trajectory but remained below the suppression threshold within the tested range, reaching a first epidemic year of approximately 92 years at 800 vaccinations per year. Both curves exhibit a nonlinear dose-response, with steeply accelerating delays in epidemic onset starting beyond roughly 300 vaccinations per year (see Table B.1 for sensitivity values).

In contrast, the two second-dose catch-up strategies ($\delta_{D_1}, \delta_{D_2}$) produced effectively no change in the first epidemic year across the entire range tested. Both curves remain nearly flat, rising only from $T \approx 28$ to $T \approx 30$ years. This suggests that boosting single-dose individuals to full two-dose status provides negligible additional protection at the population level under these conditions.

The toddler late first-dose strategy (δ_S) occupies an intermediate position. It produces a more linear increase in T across the full parameter range, rising from approximately 28 years to roughly 38 years at 800 vaccinations per year. Unlike the older age-group strategies, this response lacks the nonlinear acceleration required to achieve suppression within the tested range of parameter values.

Table 2: Summary of vaccination campaign effectiveness without importation nor declining vaccination. T is the first epidemic year recorded after the initial outbreak.

Strategy	**Target Group**	**Suppression Threshold**	**T at 800 vacc./yr**
δ_{C_2}	Adult first dose	∼500–550 vacc./yr	Suppressed
δ_{C_1}	Teen first dose	>800 vacc./yr	92–93 years
δ_S	Toddler first dose	>800 vacc./yr	37–38 years
δ_{D_2}	Adult second dose	Not achieved	∼30–31 years
δ_{D_1}	Teen second dose	Not achieved	∼30–31 years

3.4.2 With Declining Vaccination

When declining vaccination is introduced, the behavior shifts dramatically. Figure 8 and Table 3 show results for the same five strategies under the declining-coverage scenario. All five curves collapse toward the bottom of the plot, with first epidemic years ranging only from approximately 12–17 years across the entire parameter range. No strategy achieves suppression within 800 vaccinations per year, and the previous differences between strategies nearly vanish. The adult and teen first-dose campaigns (δ_{C_2} and δ_{C_1}), which were the most effective interventions in the fixed-coverage scenario, now show only a modest upward trend, reaching $T \approx 16$–17 years at 800 vaccinations per year. The second-dose strategies (δ_{D_1}, δ_{D_2}) and toddler catch-up (δ_S) remain nearly flat at $T \approx 12$–13 years. None of the curves exhibit accelerating delays (see Table B.2 for sensitivity values).

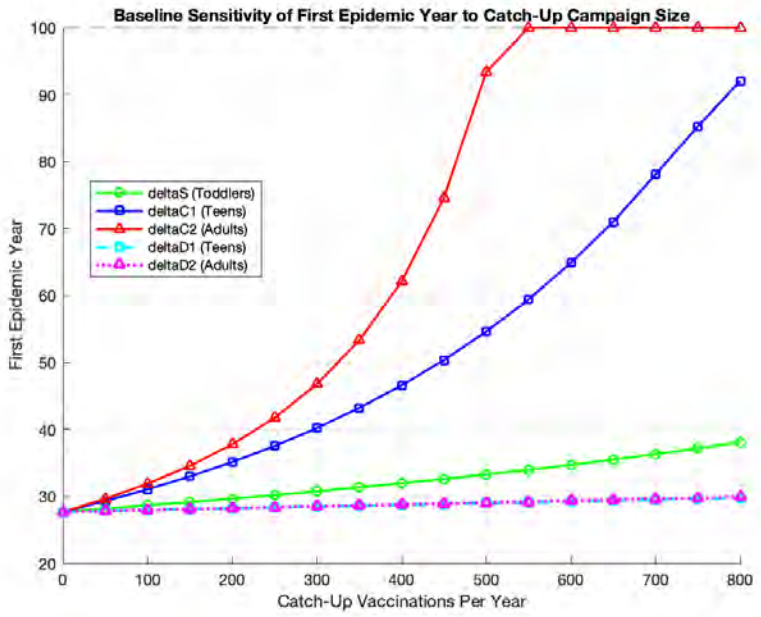

Figure 7: Sensitivity of first epidemic year, T, to catch-up campaign size across five intervention strategies, without importation nor declining vaccination. The dashed horizontal line at $T = 100$ years denotes the simulation endpoint, indicating full outbreak suppression.

Table 3: Summary of vaccination campaign effectiveness without importation, with declining vaccination. T is the first epidemic year recorded after the initial outbreak.

Strategy	Target Group	Suppression Threshold	T at 800 vacc./yr
δ_{C_2}	Adult first dose	Not achieved	∼16–17 years
δ_{C_1}	Teen first dose	Not achieved	∼16–17 years
δ_S	Toddler first dose	Not achieved	∼13–14 years
δ_{D_2}	Adult second dose	Not achieved	∼12–13 years
δ_{D_1}	Teen second dose	Not achieved	∼12–13 years

3.4.3 Increasing Routine Vaccination Coverage

Figure 9 displays the sensitivity of the first epidemic year, T, to percentage-point increases in routine first-dose coverage δ_1 (base = 92.4%) and second-dose coverage δ_2 (base = 74.2%), varied independently over the range $\{0, 0.1, 0.2, \ldots, 2.2\}$ percentage points above their baseline values.

The results mirror the asymmetry observed in the catch-up campaign analysis. Increasing δ_1 produces a strongly nonlinear delay in first epidemic year, rising from the baseline value of approximately 28 years at zero increase to full suppression after a gain of roughly 2%, which corresponds to raising first-dose coverage from 92.4% to approximately 94.4%. The response accelerates sharply above a gain of 1.0 percentage point, consistent with the system approaching the herd immunity threshold in that range. Increasing δ_2 alone produces no significant change in first epidemic year across the entire parameter range, with the curve remaining nearly flat with $T \approx 29$ at the end of the simulation. This is consistent with

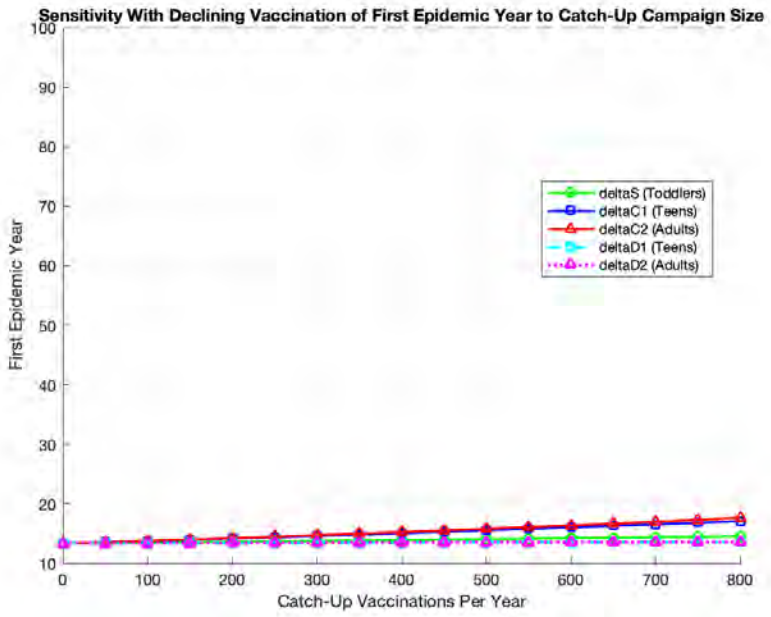

Figure 8: Sensitivity of first epidemic year, T, to catch-up campaign size across five intervention strategies, without importation but with declining vaccination. The dashed horizontal line at $T = 100$ years denotes the simulation endpoint.

the negligible effect of second-dose catch-up observed previously. Individuals already in the V-class carry sufficiently low residual susceptibility under the present parameterization that shifting additional toddlers from V_1 into R_2 via improved δ_2 coverage provides no meaningful reduction in transmission risk at the population level.

Taken together, these results identify first-dose routine coverage as the critical factor governing epidemic timing in this model. A gain of roughly two percentage points in δ_1 above the New Mexico baseline is sufficient to move the population across the elimination threshold entirely under stable conditions, while equivalent or larger improvements in δ_2 confer no additional protection.

3.4.4 Effective Reproduction Number Under Vaccination Campaign Variation

Figures 10, A.3, and A.4 show $R_e(t)$ across the full catch-up campaign variation for all five strategies, color-coded from 0 (dark blue) to 800 (yellow) vaccinations per year. These plots complement the previous first-epidemic-year analysis by showing how each strategy modifies the full temporal trajectory of R_e rather than only the timing of the first crossing.

For adult first-dose catch-up (δ_{C_2}), increasing campaign size progressively flattens the R_e trajectory, with high campaign sizes (green to yellow curves) driving R_e persistently below 1 and maintaining it there throughout the simulation horizon, which is consistent with full epidemic suppression. Teen first-dose catch-up (δ_{C_1}) produces a qualitatively similar pattern but requires a larger campaign to achieve the same persistent suppression. The toddler first-dose strategy (δ_S) produces a graded rightward shift in the R_e crossing times across the parameter range but does not drive R_e persistently below 1 at any tested campaign size. Both

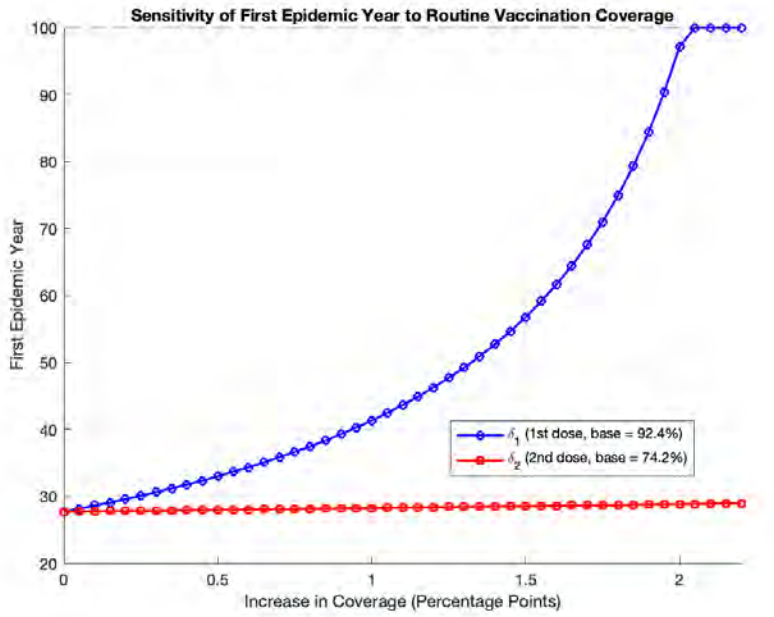

Figure 9: Sensitivity of first epidemic year, T, to percentage-point increases in routine first-dose coverage δ_1 (blue) and second-dose coverage δ_2 (red), varied independently above their 2023 New Mexico baseline values of 92.4% and 74.2% respectively. The dashed horizontal line at $T = 100$ years denotes the simulation endpoint, indicating full outbreak suppression.

second-dose strategies (δ_{D_1} and δ_{D_2}) produce trajectories that are nearly indistinguishable from the zero-campaign baseline at all campaign sizes, confirming that boosting partially-immune individuals confers no measurable reduction in transmission at the population level. These R_e trajectories are fully consistent with the first-epidemic-year results.

3.5 Dynamic Maternal Immunity

Under the dynamic $\rho(t)$ formulation, the fraction of newborns receiving maternal protection is no longer fixed but evolves continuously as a function of the adult immune composition, as described in Section 2.14. Two scenarios are examined: baseline fixed vaccination coverage and declining vaccination coverage.

3.5.1 Baseline Fixed-Coverage Scenario

Figure 11 displays the total infectious population and the corresponding $\rho(t)$ evolution side by side under the baseline fixed-coverage scenario.

Under the baseline fixed-coverage scenario, the model produces the well-separated epidemic peaks, but now each occurring approximately 3-7 years later than the fixed-ρ case. Peak infectious prevalence reaches roughly 150 individuals at the first outbreak, and declines to approximately 120 and 100 individuals during subsequent outbreaks. The long inter-epidemic interval and sharp, well-resolved peaks are consistent with a system near the herd immunity threshold, where susceptible individuals accumulate slowly between epidemic

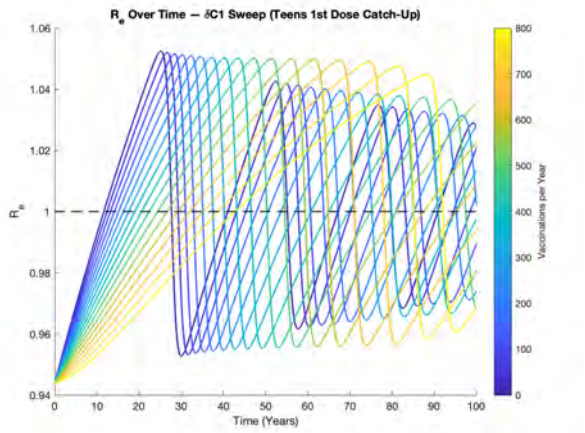

(a) Teen first-dose catch-up (δ_{C_1}). Higher campaign sizes widen the inter-epidemic interval substantially, with suppression nearly approached at the highest levels of vaccination.

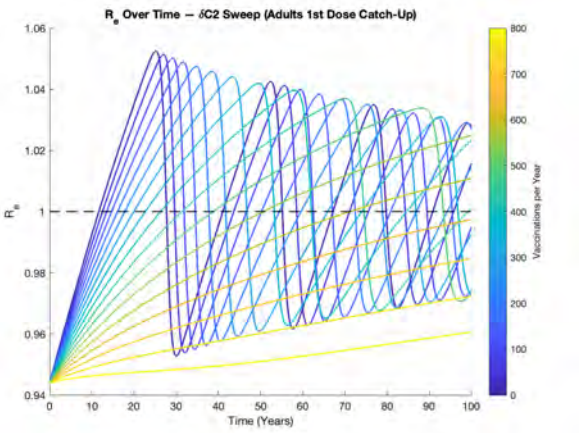

(b) Adult first-dose catch-up (δ_{C_2}). The most efficient strategy: sufficiently large campaigns drive R_e persistently below 1, maintaining elimination throughout the simulation horizon.

Figure 10: The effective reproduction number, $R_e(t)$, for teen and adult first-dose catch-up strategies across campaign sizes from 0 (dark blue) to 800 (yellow) vaccinations per year. The dashed line denotes the $R_e = 1$ threshold.

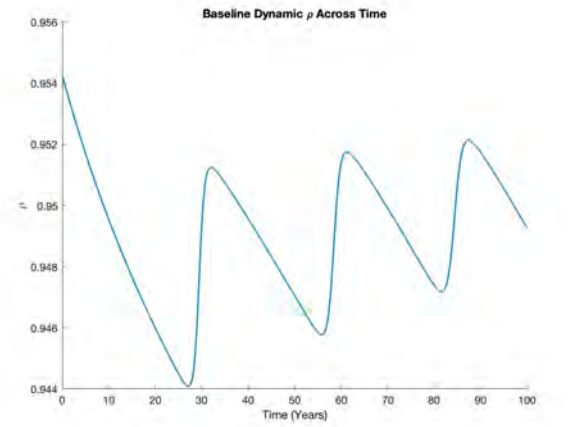

(a) Dynamic maternal immunity parameter $\rho(t)$ over 100 years. The parameter exhibits slowly increasing periodic oscillations. Notably, $\rho(t)$ declines during periods of low disease prevalence and rise following each epidemic event.

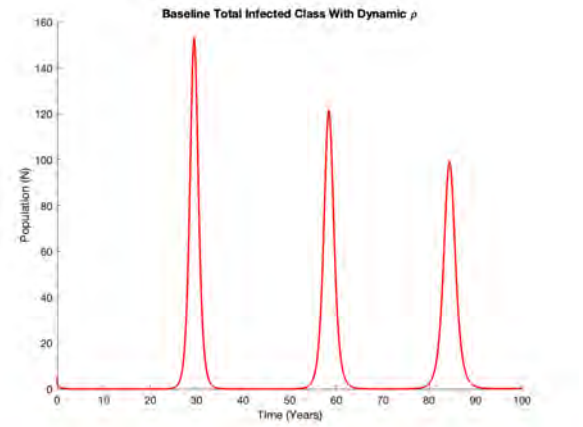

(b) Total infectious population under the baseline scenario and dynamic $\rho(t)$. Three well-separated epidemic events occur at approximately years 30, 60, and 87. Peak prevalence declines across successive outbreaks.

Figure 11: Dynamic maternal immunity parameter $\rho(t)$ and total infectious population trajectory under the baseline fixed-coverage scenario.

events before triggering the next outbreak.

The corresponding $\rho(t)$ trajectory reflects this epidemic structure directly. Beginning near 0.954, $\rho(t)$ declines gradually during each inter-epidemic period as demographic turnover slowly erodes the recovered adult pool R_3, before snapping upward sharply at each epidemic peak as a new cohort of adults passes through infection and joins R_3. The result is a slowly

increasing sawtooth oscillation bounded between approximately 0.944 and 0.954, with a period matching the epidemic interval. The small amplitude of this oscillation confirms that under stable vaccination coverage, the fraction of immune adults and, by extension, the proportion of newborns receiving maternal protection via the M_0 compartment remains essentially constant over the simulation time frame.

3.5.2 Declining Vaccination Scenario

Figure 12 displays the same pair of plots under the declining vaccination scenario, which produces a qualitatively different pattern. We obtain the same infection structure as in

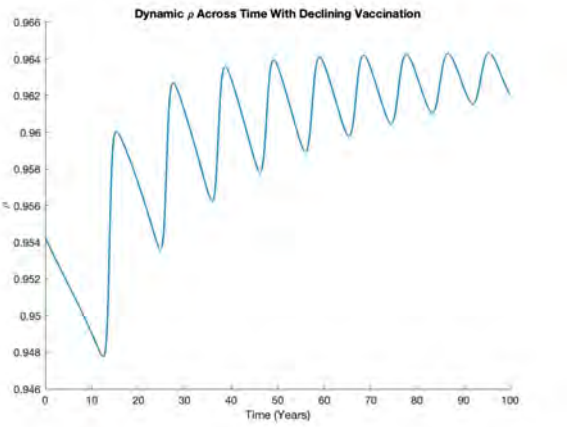

(a) Dynamic maternal immunity parameter $\rho(t)$ over 100 years.

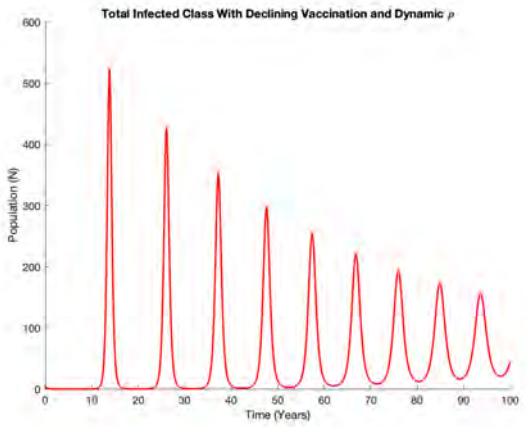

(b) Total infectious population under the declining vaccination scenario and dynamic $\rho(t)$. Peak prevalence declines across successive outbreaks.

Figure 12: Dynamic maternal immunity parameter $\rho(t)$ and total infectious population trajectory under declining vaccination. The damping and upward drift of $\rho(t)$ in the left panel is mirrored by the compression of inter-epidemic intervals in the right panel, reflecting the system's transition from epidemic to endemic dynamics driven by disease transmission rather than vaccination.

Section 3.3.1, where the first outbreak occurs much earlier, near year 12, and peak prevalence declines progressively across outbreaks. This epidemic structure explains the rise in $\rho(t)$. Following an initial trough near 0.948 at approximately year 12, driven by the first large outbreak depleting S_3 and temporarily reducing the immune adult fraction, $\rho(t)$ rises steadily as successive epidemics rapidly cycle adults through infection and into R_3, accumulating recovered immunity faster than routine vaccination decline can remove it. By year 50, $\rho(t)$ has converged near 0.963 and the oscillations have damped to a narrow band, reflecting epidemics of decreasing amplitude as the system transitions toward an endemic steady state. Under declining vaccination the disease itself becomes the dominant mechanism maintaining adult immunity and replaces the vaccine-derived protection that decays over the same time frame.

3.6 Effect of Imported Infections

To assess the sensitivity of the model to external pressure, we introduce imported infections via the κ_k terms in the I_2 and I_3 equations (see Equations 15 & 20), parameterized as $\kappa_k = n_k/(365 \cdot \tau_k)$ where n_k is the number of imported cases and τ_k is the average interval in years between importation events. New Mexico is obviously not an epidemiologically closed population (the 2025 outbreak was itself seeded by an importation from Gaines County, Texas) so understanding how importation numbers and frequency affect outbreak dynamics and intervention thresholds is essential for interpreting the robustness of the results in Sections 3.3–3.5.

3.6.1 Baseline Fixed-Coverage with Importation

We choose $n_2 = n_3 = 1$ individual, $\tau_2 = 1$ year and $\tau_3 = 2$ years (one imported teen per year, one imported adult per two years) as a plausible scenario. Figure 13 shows the total infectious class trajectory and cumulative cases under this scenario alongside the no-importation baseline.

The selected importation rate is sufficient to eliminate the large discrete epidemic peaks seen in the no-importation baseline entirely. Rather than the sharp 27-year outbreak cycle driven by susceptible accumulation, the system under importation settles into a persistent low-level endemic oscillation almost immediately, with peak prevalence remaining below 12 individuals across all age groups throughout the 100-year horizon. The adult compartment I_3 carries the largest endemic burden, followed by I_2. This endemic suppression of large outbreaks, however, does not imply a reduction in total disease burden. The cumulative case plot shows that by year 100, the imported-case scenario accumulates substantially more cases than the no-importation baseline in all age groups, as continuous endemic transmission replaces the discrete but widely spaced baseline outbreaks. The adult cumulative burden C_3 reaches approximately 39,000 cases by year 100 under importation, compared to roughly 35,000 in the baseline, while C_1 and C_2 grow more continuously rather than in discrete steps.

3.6.2 Declining Vaccination with Importation

Figure 14 compares the total infectious class trajectory and cumulative cases with and without importation under the declining vaccination scenario of Section 3.3. Under declining vaccination, the system is already transitioning toward endemic dynamics, and the addition of importation has a comparatively modest effect on the qualitative epidemic structure relative to the baseline scenario. In the importation scenario, the large epidemic peaks observed under the no-importation declining-coverage conditions persist. However, the intervals between these epidemics become even shorter. This occurs because imported cases trigger outbreaks slightly earlier than they would have arisen from solely the buildup of the susceptible population. Both trajectories settle into endemic behavior, though the no-importation scenario (red) consistently produces larger peak prevalence throughout, as importation-triggered outbreaks deplete the susceptible pool earlier and prevent the full accumulation that drives the larger no-importation peaks. The with-importation and no-importation cumulative case curves are nearly overlapping throughout the 100-year horizon, with the largest absolute difference appearing in C_2 and C_3 during the early outbreak years. This convergence supports

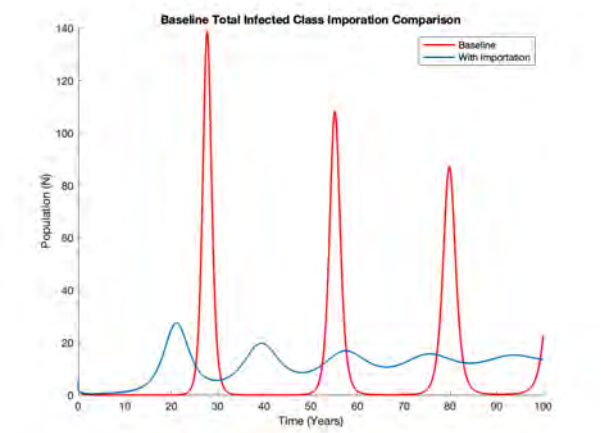

(a) Total infectious class under baseline coverage with importation ($n_{2,3} = 1$,$\tau_2 = 1$ yr, $\tau_3 = 2$ yr). Large epidemic peaks are replaced by persistent low-level endemic oscillation below 20 individuals.

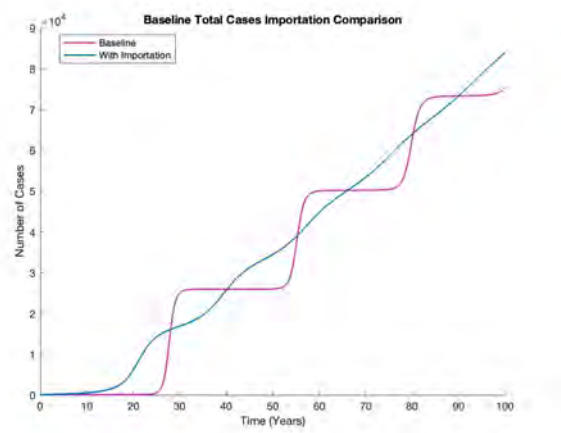

(b) Cumulative cases C_k under baseline coverage with importation. Continuous accumulation replaces the staircase pattern, with C_3 reaching approximately 39,000 by year 100.

Figure 13: Infectious class and cumulative cases under baseline fixed-coverage with importation ($\tau_2 = 1$, $\tau_3 = 2$ yr).

the conclusion that under declining vaccination, internal transmission dynamics dominate and importation is not the primary driver of long-run disease burden.

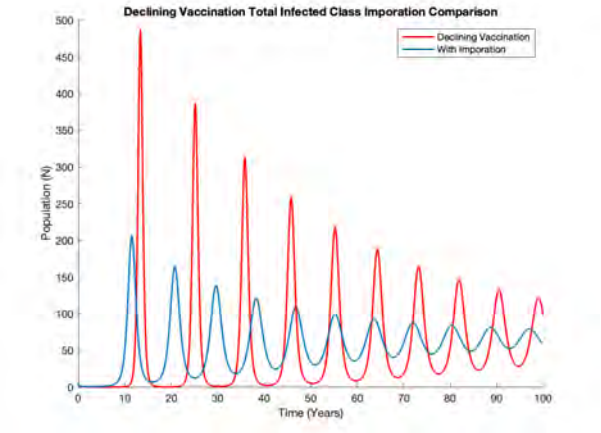

(a) Total infectious class I with (blue) and without (red) importation under declining vaccination.

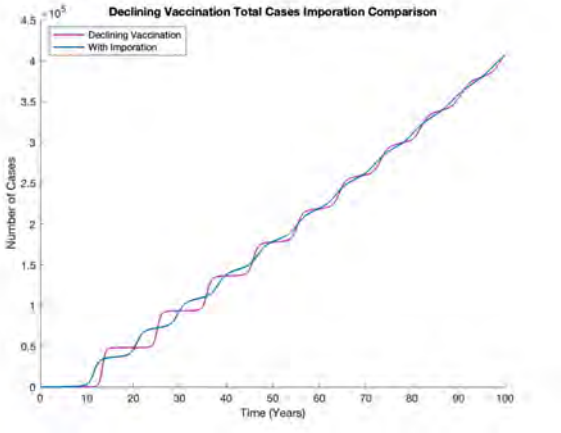

(b) Cumulative cases with (blue) and without (pink) importation under declining vaccination. Curves are nearly overlapping throughout.

Figure 14: Infectious class and cumulative cases under declining vaccination with and without importation.

3.6.3 Effect on Catch-Up Vaccination Campaigns & Increasing Routine Coverage

Under importation, the large discrete epidemic peaks that defined the first-epidemic-year outcome variable T in Section 2.13 are more distorted and endemic. This makes T an unsuitable summary for comparing campaign effectiveness. Instead, we visualize the full $I_{\text{total}}(t)$ trajectory across routine coverage and the campaign variation for each strategy, which directly shows how the infectious burden evolves over time as a function of vaccination intensity. Figures 15, A.5, A.6, and A.7 show these trajectories for all five strategies and routine coverage, color-coded by campaign size from 0 (dark blue) to 800 (yellow) vaccinations per year, and by routine dose percent increase from 0% (dark blue) to 3% (yellow).

The qualitative ranking of strategies established in Section 3.4.1 is preserved under importation. Adult first-dose catch-up (δ_{C_2}) remains the most efficient intervention, since at sufficiently high campaign sizes (green curves), $I_{\text{total}}(t)$ is driven toward near-zero and remains there throughout the simulation, indicating effective suppression of both importation-seeded endemic transmission and any residual epidemic pressure. Teen first-dose catch-up (δ_{C_1}) produces a similar pattern but requires a larger campaign to achieve the same suppression. The toddler first-dose strategy (δ_S) produces a graded reduction in the endemic level across the parameter range but does not achieve suppression at any tested campaign size. Both second-dose strategies (δ_{D_1} and δ_{D_2}) produce trajectories indifferent from the zero-campaign baseline at all campaign sizes.

In terms of routine vaccination, δ_1 increases to full suppression after a gain of roughly 2.5%, which corresponds to raising first-dose coverage from 92.4% to nearly 95%, consistent with the herd-immunity threshold for measles. Increasing δ_2 alone produces no significant change. The robustness of this ranking across importation scenarios strengthens the conclusion that first-dose adult catch-up vaccination is the most effective, aside from increasing first-dose routine vaccination.

3.6.4 Dynamic Maternal Immunity with Importation

Figure A.8 displays $\rho(t)$ under both the baseline fixed-coverage and declining vaccination scenarios, comparing the no-importation trajectories against the corresponding importation scenarios. Under baseline fixed coverage, the two trajectories are indistinguishable during the first $\sim$10 years as $\rho(t)$ declines from its initial value of approximately 0.954. Beyond year 15, the two curves diverge. Under importation, the continuous low-level endemic transmission prevents the extreme susceptible accumulation that drives these large oscillations. Instead, $\rho(t)$ damps toward a narrow, relatively stable band near 0.950 after year 40. This means that while importation suppresses the large discrete epidemic peaks, it simultaneously eliminates the periodic refreshing of maternal immunity that those peaks generate. This results in a more consistent but lower peak maternal immunity level compared to the outbreak-driven spikes of the no-importation case.

Under declining vaccination, the importation (red) and no-importation (blue) $\rho(t)$ trajectories are nearly indistinguishable throughout the full 100-year horizon. Both curves trough near 0.948–0.950 at approximately year 12 as the first large outbreak temporarily depletes the adult immune fraction. They then rise together in a pattern of compressing oscilla-

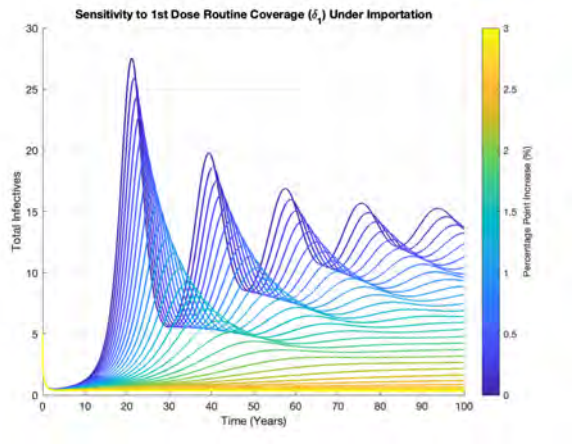

(a) Sensitivity of total infectives to percentage-point increases in first-dose routine coverage δ_1 under importation. A gain of roughly 2.5% is enough to suppress future epidemics.

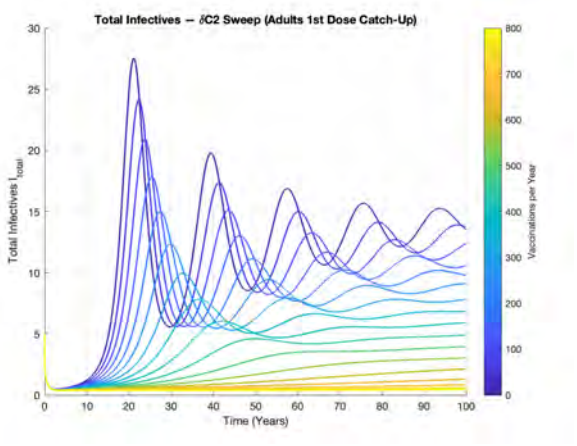

(b) Adult first-dose catch-up (δ_{C_2}). The most efficient strategy: high campaign sizes drive I_{total} to near-zero and maintain suppression throughout the horizon.

Figure 15: $I_{\text{total}}(t)$ across variation in routine first-dose coverage δ_1 (left) and adult catch-up δ_{C_2} (right) under importation. Both strategies focus on increasing first-dose immunity, showing substantial impacts on epidemic suppression compared to the baseline.

tions before converging toward a narrow band near 0.963 by the end of the simulation. In this scenario, internal transmission dynamics are so dominant that the additional pressure from importation contributes negligible perturbation to the adult immune composition. The convergence of both curves to the same value confirms that under declining vaccination, the long-run maternal immunity level is determined almost entirely by the high intensity of internal endemic transmission.

4 Discussion

This study developed and analyzed an age-structured SEIR-MV compartmental model of measles transmission parameterized to the New Mexico population. The model incorporated time-varying vaccination coverage, waning maternal antibodies, targeted catch-up campaigns, and imported infections to address how continued declines in routine immunization, combined with age-structured immunity and intervention strategies, will shape future outbreak dynamics.

4.1 Principal Findings

Under current fixed NM vaccination coverage, the model reproduces long inter-epidemic intervals of approximately 27–28 years, with the initial transient dynamics producing a case distribution that closely approximates the 2025 New Mexico outbreak. The effective reproduction number R_e begins near 0.94 at $t = 0$ and oscillates around the elimination threshold of 1, crossing above 1 roughly a decade before each major outbreak and dropping sharply afterward as susceptible individuals are depleted. This sawtooth pattern in R_e

sustains the characteristic long inactive periods between epidemics while keeping the system near, but not safely below, the herd immunity threshold.

When routine coverage declines at 0.9 percentage points for the first decade (consistent with observed global two-dose trends), dynamics shift dramatically. The first outbreak advances to approximately year 12, peak infectious prevalence rises roughly three-fold, R_e crossings of 1 occur earlier and more frequently, and the system transitions from discrete epidemic cycling to sustained endemic transmission by mid-century, with oscillations damping toward a narrow band centered near $R_e = 1$. Cumulative burden increases by an order of magnitude over 100 years relative to the baseline, with adults and older children/teenagers continuing to drive the majority of cases.

Sensitivity analyses demonstrate distinguishable results for catch-up campaign efficacy and routine vaccination. Under stable coverage, adult first-dose catch-up campaigns (δ_{C_2}) result as the most efficient supplementary strategy, achieving full epidemic suppression (simulation endpoint of 100 years with R_e persistently below 1) at approximately 500-550 vaccinations per year. Teen first-dose catch-up follows a similar but less efficient trajectory. In contrast, second-dose boosting of partially immune individuals (δ_{D_1}, δ_{D_2}) produces negligible impact on either first epidemic year or R_e trajectories across the full range tested. This reflects the low residual susceptibility ($\varepsilon = 0.07$) already conferred by a single dose. Toddler late first-dose catch-up occupies an intermediate position but does not achieve suppression within our tested range of 800 vaccinations per year. Increasing routine coverage confirms the same pattern: raising first-dose coverage δ_1 by roughly 2.0 percentage points (to 94.4%) suffices for full suppression, while equivalent gains in second-dose coverage δ_2 result in no measurable benefit.

Under declining vaccination, no catch-up strategy achieves suppression within the tested range; all produce only modest delays, with first epidemic years clustering between approximately 12–17 years. This underscores that targeted campaigns cannot substitute for sustained routine immunization, as they fail to counteract the continuous influx of susceptibles from eroding birth-cohort coverage. The role of catch-up vaccination therefore shifts from epidemic suppression to epidemic delay, and must be viewed as a complement to, not a replacement for, maintaining routine immunization above the herd immunity threshold.

Dynamic maternal immunity analysis reveals a slower but important feedback. With fixed coverage, $\rho(t)$ oscillates narrowly between approximately 0.944 and 0.954 driven by the epidemic cycle. This declines gradually during inter-epidemic periods as demographic turnover erodes the recovered adult pool, then snapping upward at each outbreak as a new cohort of adults passes through infection and joins R_3. Under declining coverage, disease transmission increasingly dominates vaccination as the source of adult immunity. Imported infections at plausible low-level rates eliminate large discrete peaks under fixed coverage. Importations convert the system to low-amplitude endemic transmission and damping $\rho(t)$ to a narrow stable band near 0.950, but have minimal additional effect under declining coverage where internal dynamics already dominate. In both the baseline and declining vaccination scenarios, the dynamic $\rho(t)$ formulation produces infection curves qualitatively similar to their fixed-ρ counterparts, with epidemic peaks shifted by at most a few years and no change in the number of outbreaks or long-run endemic behavior. The value of the dynamic formulation lies not in altering the infection trajectory but in revealing the feedback between adult immune composition and newborn protection, which is a mechanism invisible

to a static parameterization.

The imported infection analysis confirms that even low-frequency importation (one teen case per year and one adult case every two years) suffices to eliminate the discrete epidemic cycle under fixed coverage and convert the system to persistent endemic transmission, while simultaneously increasing long-run cumulative burden. Under this scenario, $\rho(t)$ damps to a narrow flat band near 0.950 rather than oscillating through large sawtooth cycles. This is due to continuous low-level endemic transmission preventing the susceptible accumulation needed to drive the large outbreak-driven spikes that characterize the no-importation case. Under declining vaccination, importation has comparatively little additional effect on either epidemic dynamics or maternal protection. The suppression threshold for routine first-dose coverage δ_1 shifts upward from approximately 2.0 percentage points above the New Mexico baseline in the no-importation setting to approximately 2.5 percentage points under importation, corresponding to raising δ_1 from 92.4% to just under 95%. This shift directly reflects the additional transmission pressure introduced by importation and is consistent with the widely cited 93–95% herd immunity threshold for measles [19]. Closing the gap between current New Mexico coverage and this threshold is precisely what is required to maintain elimination even in the presence of ongoing external seeding. The robustness of the catch-up vaccination strategy rankings across both importation scenarios strengthens confidence in the policy conclusion that adult first-dose catch-up is the most efficient supplementary intervention.

4.2 Parameterization Challenges and Limitations

The most significant parameterization challenge in this project was the construction of the WAIFW transmission matrix $\boldsymbol{\beta}$. Age-specific contact rates for measles transmission in New Mexico are not directly observed in contemporary data. The matrix was therefore estimated from historical case notification data. The reliance on data that may not reflect current social mixing patterns, including shifts in household composition, school attendance, and population age structure, introduces uncertainty that cannot be fully resolved without modern contact survey data specific to New Mexico or the broader US Southwest. The scaling factor of 1.112 remains an approximation, and future work should aim to reduce the uncertainty for this parameter.

A related structural limitation is the use of time-invariant transmission rates throughout the simulation. Real measles transmission is strongly seasonal, driven by school-term aggregation of children in the primary transmission age groups. The present model's four broad age groups, particularly the 5–19 year cohort spanning late childhood through adolescence, creates a more generalized age boundary preventing a more accurate representation of school-driven contact patterns. A natural extension would subdivide the school-age group into narrower cohorts aligned with school enrollment transitions, and incorporate temporal forcing of the within-group transmission rates β_{22} to reflect seasonal variation in school-age contact intensity. Such modifications would likely produce the annual or biennial epidemic cycles characteristic of measles in school-age populations, and would more faithfully represent the role of school holidays in shaping outbreak timing [4].

A further limitation concerns the scope of the sensitivity analysis presented here. The current analysis varies catch-up vaccination rates in isolation, while holding all other pa-

rameters fixed at their point estimates. A full global sensitivity analysis over the other parameters has not yet been performed. Given that several results depend strongly on specific parameter values, particularly the ε parameter governing the residual susceptibility of V-class individuals and the 0.9 percentage-point-per-year decline rate used to model coverage erosion, a full sensitivity analysis represents an important next step. Such an analysis would also include the birth and death parameters, and the initial conditions for the adult susceptible and vaccinated compartments, whose values carry meaningful uncertainty under the redistribution assumptions described in Section 2.10.

The model also incorporates several other structural simplifications that may affect its quantitative predictions. It does not distinguish sex, geographic subregion within New Mexico, or community-level clustering, all of which were epidemiologically important in the 2025 outbreak. That outbreak originated in a spatially and socially concentrated unvaccinated Mennonite community before spreading more broadly, a dynamic that the compartmental framework employed here cannot represent. Modeling such community-level heterogeneity would require individual-based or network-structured models going beyond the present approach.

The use of a single population-averaged case fatality ratio $p = 0.001$ also requires further inspection. Measles mortality is strongly age-dependent and is substantially elevated in infants and immunocompromised individuals. The New Mexico context includes populations, such as young children in under-resourced rural communities, who may face higher fatality risks than this uniform estimate reflects. The single-value parameterization likely underestimates mortality in the youngest age groups, while slightly overestimating it in the school-age group [21].

Finally, the deterministic framework employed here cannot capture the stochastic extinction events that are epidemiologically important when infectious prevalence is low, particularly during the long inter-epidemic troughs characteristic of the baseline scenario. A natural extension would reformulate the model as a continuous-time stochastic system, which would better characterize the role of chance in determining whether a small importation event seeds a major outbreak or dies out.

4.3 Implications for Vaccine Skepticism and Communication

The results of this model must be understood against the history of the vaccine hesitancy landscape that contributed to the 2025 New Mexico and Texas outbreaks. A significant driver of MMR refusal in the United States has been the now-retracted 1998 *Lancet* paper by Andrew Wakefield, which falsely claimed a causal link between the MMR vaccine and autism spectrum disorder. Despite the paper's retraction, Wakefield's subsequent public campaign sustained measurable levels of vaccine hesitancy among certain communities for over two decades [22]. The Gaines County outbreak cluster, concentrated in a home-schooled and religiously observant population with first-dose coverage of only 81%, is a direct consequence of the susceptible pockets created by sustained hesitancy. The model's sensitivity analyses demonstrate that relatively small reductions in routine coverage, far short of complete refusal by any community, can substantially advance outbreak timing and increase peak burden. The finding that raising δ_1 by at least two percentage points eliminates all major outbreaks beyond the initial transient demonstrates how a small increase in first-dose

coverage above the New Mexico baseline would suffice to move the population across the elimination threshold entirely.

4.4 Conclusion

This study demonstrates that continued decline in measles vaccination coverage at rates observed globally since 2019 is projected to fundamentally transform the epidemic landscape in New Mexico. Outbreak onset advances by roughly 15 years relative to stable-coverage projections, peak burden amplifies, and the system transitions from episodic epidemic cycling to endemic transmission in an earlier time frame. Targeted catch-up vaccination can delay outbreaks under stable coverage conditions, and adult first-dose catch-up is consistently the most efficient single intervention across all scenarios tested. No catch-up strategy tested here can compensate for an ongoing erosion of routine vaccination. The dynamic maternal immunity analysis demonstrates how, under declining coverage, disease transmission rather than vaccination becomes the primary mechanism sustaining adult and therefore maternal immunity. These findings support the prioritization of two complementary actions: restoring and sustaining routine MMR coverage above the 93–95% herd immunity threshold in all age cohorts, and deploying first-dose catch-up campaigns directed at susceptible adults as the highest-yield supplementary intervention when resources are limited. Future work should pursue a full multi-parameter global sensitivity analysis of the model's outputs with respect to uncertain inputs. Structural extensions incorporating narrower school-age cohorts and seasonal temporal forcing of transmission rates would also improve the model's ability to capture the school-term-driven epidemic cycles characteristic of measles, and would better position the framework for school-level or county-level policy analysis in New Mexico.

References

[1] Measles Outbreak - 2025 information.

[2] Haileyesus Tessema Alemneh and Asnakew Mesele Belay. Modelling, Analysis, and Simulation of Measles Disease Transmission Dynamics. *Discrete Dynamics in Nature and Society*, 2023(1):9353540, 2023. _eprint: https://onlinelibrary.wiley.com/doi/pdf/10.1155/2023/9353540.

[3] Ottar N. Bjørnstad, Katriona Shea, Martin Krzywinski, and Naomi Altman. Modeling infectious epidemics. *Nature Methods*, 17(5):455–456, May 2020.

[4] Benjamin Bolker. Chaos and complexity in measles models: A comparative numerical study. *Mathematical Medicine and Biology*, 10(2):83–95, 1993.

[5] CDC. Clinical Overview of Measles, March 2026.

[6] CDC. Measles Vaccine Recommendations, March 2026.

[7] O. Diekmann, J. A. P. Heesterbeek, and M. G. Roberts. The construction of next-generation matrices for compartmental epidemic models. *Journal of the Royal Society Interface*, 7(47):873–885, June 2010.

[8] Owen Dyer. Measles: Texas outbreak spreads to New Mexico. *BMJ*, 388:r357, February 2025.

[9] B. T. Grenfell and R. M. Anderson. Pertussis in England and Wales: an investigation of transmission dynamics and control by mass vaccination. *Proceedings of the Royal Society of London. Series B, Biological Sciences*, 236(1284):213–252, April 1989.

[10] Fiona M. Guerra, Shelly Bolotin, Gillian Lim, Jane Heffernan, Shelley L. Deeks, Ye Li, and Natasha S. Crowcroft. The basic reproduction number (R0) of measles: a systematic review. *The Lancet Infectious Diseases*, 17(12):e420–e428, December 2017.

[11] Joseph Leonardo Marvin Hamzah, Helisyah Nur Fadhilah, and Rindra Syaifullah. Analysis of the SEIR Model for Measles Spread with the Influence of Vaccination. *IAENG International Journal of Applied Mathematics*, 55(3):626–635, March 2025. Num Pages: 626-635.

[12] Herbert W. Hethcote. The Mathematics of Infectious Diseases. *SIAM Review*, 42(4):599–653, January 2000.

[13] Yingze Hou and Hoda Bidkhori. Multi-feature SEIR model for epidemic analysis and vaccine prioritization. *PLOS ONE*, 19(3):e0298932, March 2024.

[14] Elizabeth Hunter and John D. Kelleher. Understanding the assumptions of an SEIR compartmental model using agentization and a complexity hierarchy. *Journal of Computational Mathematics and Data Science*, 4:100056, August 2022.

[15] Matt J. Keeling and Pejman Rohani. *Modeling Infectious Diseases in Humans and Animals*. Princeton University Press, September 2011. Google-Books-ID: LxzILSuKDhUC.

[16] William Ogilvy Kermack and A. G. McKendrick. A contribution to the mathematical theory of epidemics. *Proceedings of the Royal Society of London. Series A, Containing Papers of a Mathematical and Physical Character*, 115(772):700–721, August 1927.

[17] Mathew V. Kiang, Kate M. Bubar, Yvonne Maldonado, Peter J. Hotez, and Nathan C. Lo. Modeling Reemergence of Vaccine-Eliminated Infectious Diseases Under Declining Vaccination in the US. *JAMA*, 333(24):2176–2187, June 2025.

[18] A. R. McLean and R. M. Anderson. Measles in Developing Countries. Part II. The Predicted Impact of Mass Vaccination. *Epidemiology and Infection*, 100(3):419–442, 1988.

[19] Abhishek Pandey and Alison P. Galvani. Exacerbation of measles mortality by vaccine hesitancy worldwide. *The Lancet Global Health*, 11(4):e478–e479, April 2023.

[20] Pedro Plans-Rubió. Measles Vaccination Coverage and Anti-Measles Herd Immunity Levels in the World and WHO Regions Worsened from 2019 to 2023. *Vaccines*, 13(2):157, February 2025.

[21] Allison Portnoy, Mark Jit, Matthew Ferrari, Matthew Hanson, Logan Brenzel, and Stéphane Verguet. Estimates of case-fatality ratios of measles in low-income and middle-income countries: a systematic review and modelling analysis. *The Lancet. Global Health*, 7(4):e472–e481, February 2019.

[22] T. S. Sathyanarayana Rao and Chittaranjan Andrade. The MMR vaccine and autism: Sensation, refutation, retraction, and fraud. *Indian Journal of Psychiatry*, 53(2):95–96, 2011.

[23] D. Schenzle. An age-structured model of pre- and post-vaccination measles transmission. *IMA journal of mathematics applied in medicine and biology*, 1(2):169–191, 1984.

Appendix

Supplementary Figures

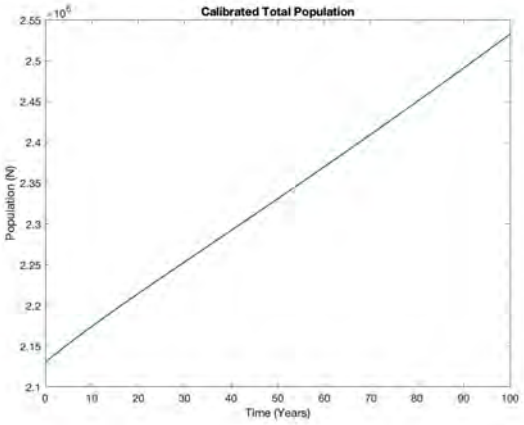

(a) Total population $N(t)$ over 100 years. Starting near 2.13 million (consistent with 2023 New Mexico census estimates), $N(t)$ grows approximately linearly to roughly 2.53 million by year 100.

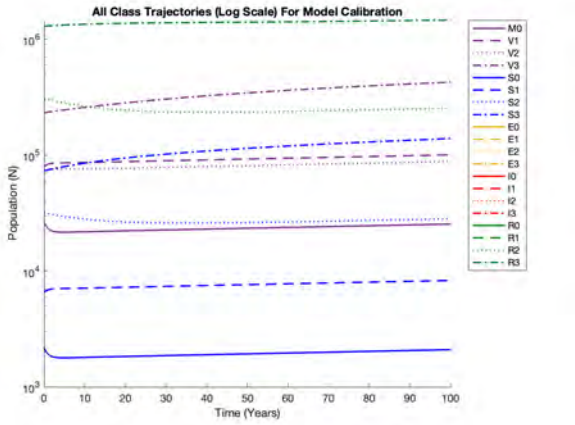

(b) All compartment trajectories on a log scale over 100 years with infection disabled. All E_k and I_k compartments remain identically at zero throughout, confirming no transmission arises from the demographic or vaccination structure alone.

Figure A.1: Total population and all-class log-scale trajectories under the no-infection calibration run. The linear population growth and smooth monotone compartment behavior confirm that the demographic and vaccination parameters are correctly specified.

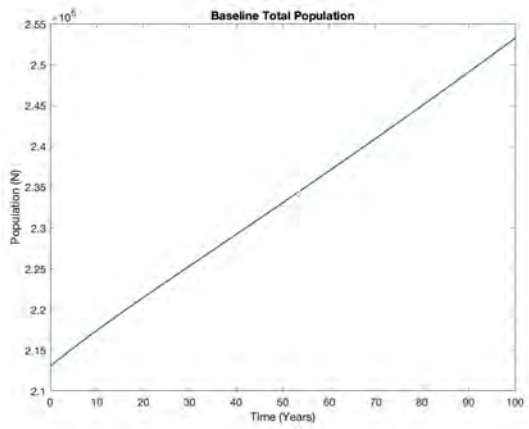

(a) Total population $N(t)$ over 100 years. Growth remains approximately linear from 2.13 million to 2.53 million, consistent with New Mexico's net positive birth rate. The elevated disease burden under baseline conditions does not perturb demographic dynamics.

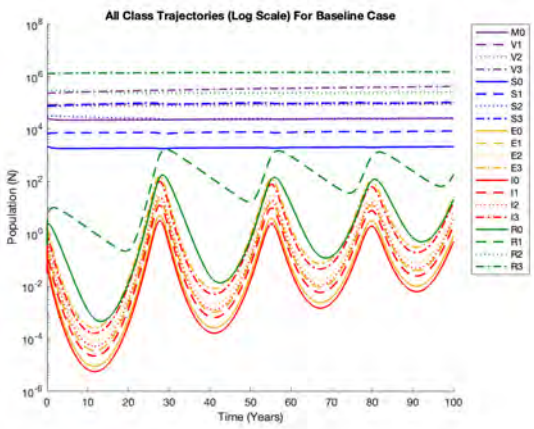

(b) All compartment trajectories on a log scale over 100 years under baseline conditions. The three epidemic events at approximately years 28, 55, and 80 are visible as synchronized oscillations across all E_k and I_k compartments, while the demographic compartments remain comparatively stable.

Figure A.2: Total population and all-class log-scale trajectories under baseline conditions over 100 years. The log scale reveals the full dynamic range of the epidemic signal across all compartments simultaneously.

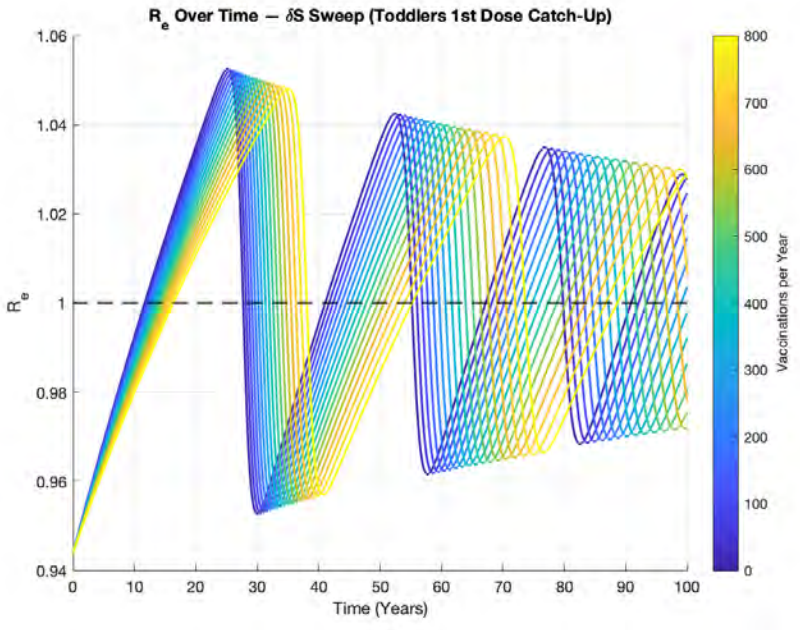

Figure A.3: $R_e(t)$ across variations in toddler first-dose catch-up (δ_S) for campaign sizes from 0 (dark blue) to 800 (yellow) vaccinations per year. The dashed line denotes the $R_e = 1$ threshold. Increasing campaign size progressively delays R_e crossings but does not achieve persistent suppression below 1 within the tested range.

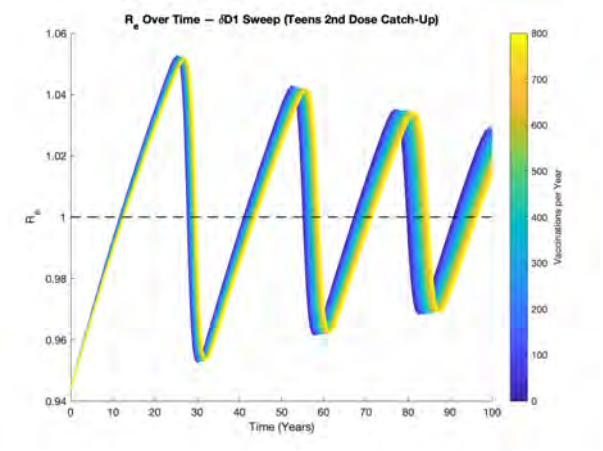

(a) Teen second-dose catch-up (δ_{D_1}). All curves collapse to a single trajectory indistinguishable from the zero-campaign baseline, confirming no effect on R_e at any tested campaign size.

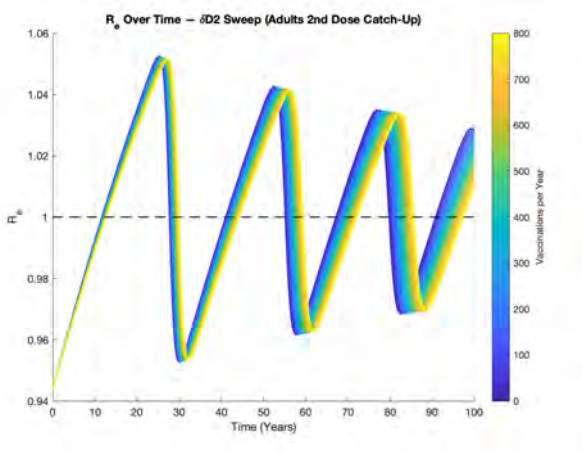

(b) Adult second-dose catch-up (δ_{D_2}). As with δ_{D_1}, all campaign sizes collapse to a single trajectory with no measurable impact on R_e.

Figure A.4: $R_e(t)$ across variations in teen and adult second-dose catch-up strategies for campaign sizes from 0 (dark blue) to 800 (yellow) vaccinations per year. Both strategies are ineffective at all tested campaign sizes.

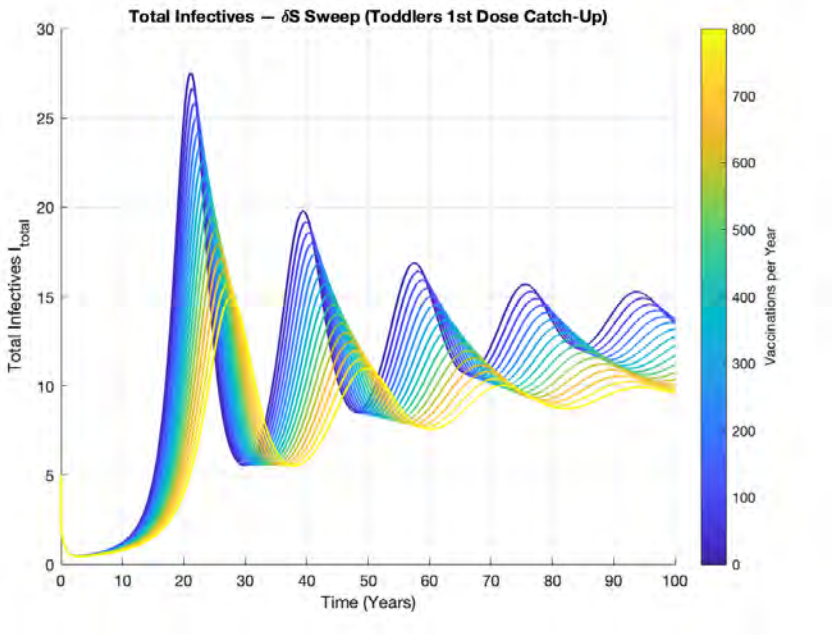

Figure A.5: $I_{\text{total}}(t)$ across variations in toddler first-dose catch-up (δ_S) under importation. Graded reduction in endemic level across campaign sizes but no suppression achieved within the tested range.

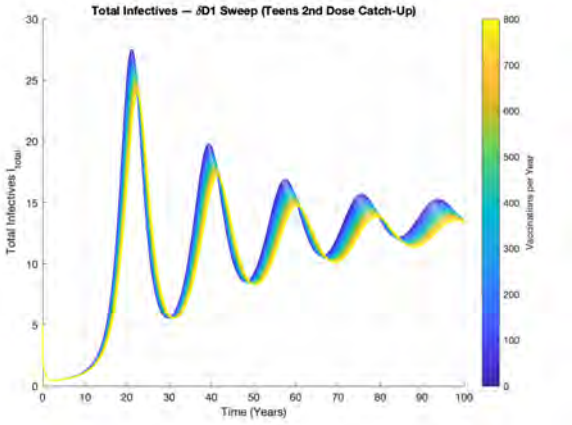

(a) Teen second-dose catch-up (δ_{D_1}) under importation.

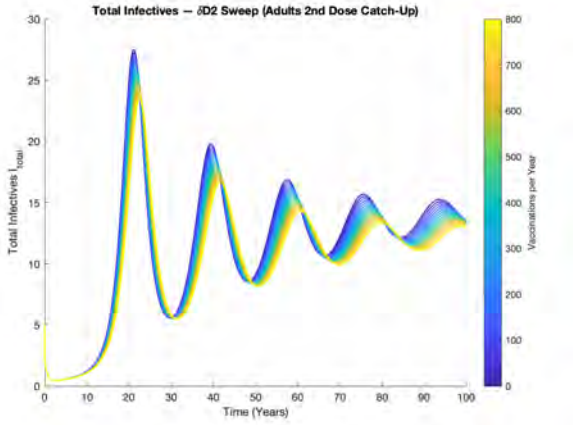

(b) Adult second-dose catch-up (δ_{D_2}) under importation. As with δ_{D_1}, no measurable impact on infectious under importation.

Figure A.6: $I_{\text{total}}(t)$ across variation in teen and adult second-dose catch-up strategies under importation. Both strategies are ineffective at all tested campaign sizes.

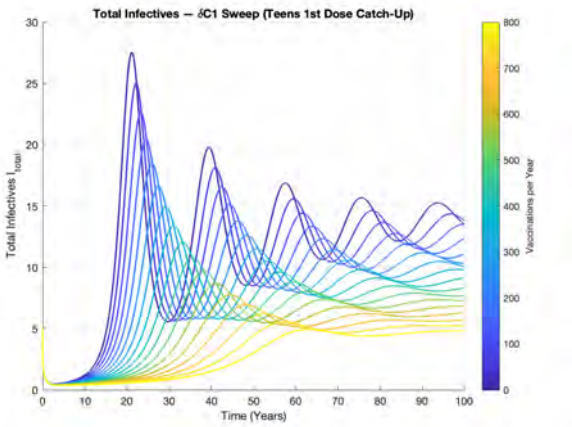

(a) Teen first-dose catch-up (δ_{C_1}). Higher campaign sizes progressively eliminate epidemic peaks and reduce the endemic floor, with suppression approached at the upper end of the parameter range.

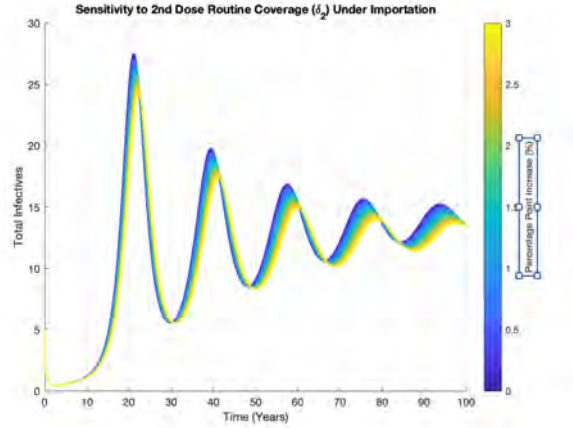

(b) Sensitivity of $I_{\text{total}}(t)$ to percentage-point increases in second-dose routine coverage δ_2 under importation. All curves are nearly indistinguishable across the full parameter range.

Figure A.7: $I_{\text{total}}(t)$ across variation in teen catch-up δ_{C_1} (left) and second-dose routine coverage δ_2 (right) under importation. While teen catch-up shows a clear dose-response relationship, the second-dose improvements remain negligible in their effect on overall transmission.

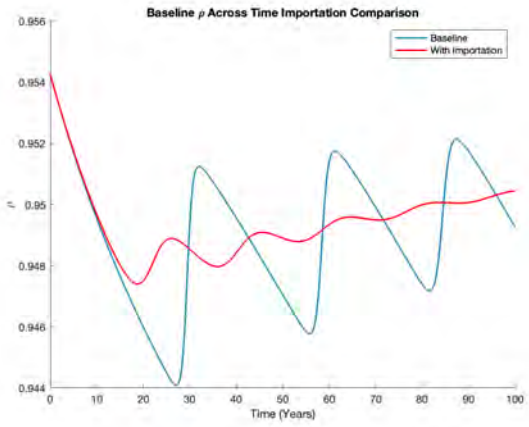

(a) Baseline fixed-coverage scenario. The no-importation curve (blue) oscillates in large sawtooth cycles between approximately 0.944 and 0.952

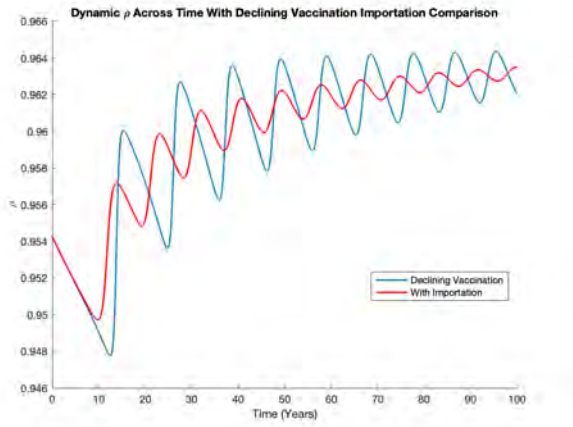

(b) Declining vaccination scenario. Both curves trough near 0.948–0.950 at year 12 before rising together to converge near 0.963 by year 100.

Figure A.8: Dynamic maternal immunity parameter $\rho(t)$ with and without importation under baseline fixed coverage (left) and declining vaccination (right). Importation damps the oscillatory structure of $\rho(t)$ under stable coverage but has negligible effect under declining vaccination, where internal transmission dynamics dominate.

Supplementary Tables

Table B.1: Local sensitivity $\Delta T/\Delta n$ (years per vaccination per year) of first epidemic year to catch-up campaign size, without importation nor declining vaccination.

Range (vax/yr)	δ_S	δ_{C_1}	δ_{C_2}	δ_{D_1}	δ_{D_2}
0–50	0.01003	0.03244	0.03863	0.00279	0.00279
50–100	0.00953	0.03474	0.04532	0.00274	0.00274
100–150	0.00937	0.03858	0.05353	0.00285	0.00285
150–200	0.01025	0.04290	0.06389	0.00225	0.00225
200–250	0.01118	0.04789	0.07912	0.00263	0.00329
250–300	0.01063	0.05370	0.10104	0.00290	0.00285
300–350	0.01211	0.06022	0.13041	0.00214	0.00279
350–400	0.01233	0.06718	0.17573	0.00230	0.00214
400–450	0.01249	0.07551	0.25063	0.00274	0.00285
450–500	0.01397	0.08499	0.37545	0.00279	0.00290
500–550	0.01342	0.09627	0.13227	0.00225	0.00274
550–600	0.01496	0.10910	0.00000	0.00241	0.00279
600–650	0.01584	0.12318	0.00000	0.00268	0.00285
650–700	0.01611	0.14093	0.00000	0.00236	0.00279
700–750	0.01748	0.14362	0.00000	0.00279	0.00274
750–800	0.01786	0.13584	0.00000	0.00274	0.00340

Table B.2: Local sensitivity $\Delta T/\Delta n$ (years per vaccination per year) of first epidemic year to catch-up campaign size, without importation but with declining vaccination.

Range (vax/yr)	δ_S	δ_{C_1}	δ_{C_2}	δ_{D_1}	δ_{D_2}
0–50	0.00148	0.00395	0.00438	0.00055	0.00055
50–100	0.00126	0.00438	0.00460	0.00005	0.00005
100–150	0.00121	0.00384	0.00433	0.00044	0.00000
150–200	0.00153	0.00455	0.00444	0.00005	0.00049
200–250	0.00159	0.00389	0.00466	0.00044	0.00044
250–300	0.00132	0.00449	0.00532	0.00044	0.00044
300–350	0.00153	0.00444	0.00515	0.00011	0.00011
350–400	0.00132	0.00460	0.00504	0.00060	0.00060
400–450	0.00153	0.00493	0.00521	0.00005	0.00005
450–500	0.00181	0.00455	0.00559	0.00060	0.00060
500–550	0.00153	0.00499	0.00597	0.00005	0.00005
550–600	0.00159	0.00504	0.00570	0.00000	0.00049
600–650	0.00132	0.00515	0.00625	0.00055	0.00005
650–700	0.00197	0.00504	0.00619	0.00044	0.00044
700–750	0.00142	0.00542	0.00619	0.00005	0.00005
750–800	0.00197	0.00515	0.00696	0.00049	0.00055